Magnetic degeneracy points in interacting two-spin systems: Geometrical patterns, topological charge distributions, and their stability

György Frank,[1] Zoltán Scherübl,[1] Szabolcs Csonka,[1] Gergely Zaránd,[2,3] and András Pályi[2,*]

[1]*Department of Physics, Budapest University of Technology and Economics and MTA-BME "Momentum" Nanoelectronics Research Group, H-1111 Budapest, Budafoki út 8., Hungary*

[2]*Department of Theoretical Physics and MTA-BME Exotic Quantum Phases "Momentum" Research Group, Budapest University of Technology and Economics, H-1111 Budapest, Hungary*

[3]*MTA-BME Quantum Correlations Group, Budapest University of Technology and Economics, H-1111 Budapest, Hungary*

(Received 24 February 2020; accepted 6 May 2020; published 5 June 2020)

Spectral degeneracies of quantum magnets are often described as diabolical points or magnetic Weyl points, which carry topological charge. Here, we study a simple, yet experimentally relevant, quantum magnet: two localized interacting electrons subject to spin-orbit coupling. In this setting, the degeneracies are not necessarily isolated points, but can also form a line or a surface. We identify 10 different possible geometrical patterns formed by these degeneracy points, and study their stability under small perturbations of the Hamiltonian. Stable structures are found to depend on the relative sign $\mathcal{S}$ of the determinants of the two g tensors. Both for $\mathcal{S}=+1$ and -1, two stable configurations are found, and three out of these four configurations are formed by pairs of Weyl points. These stable regions are separated by a surface of almost stable configurations, with a structure akin to codimension-one bifurcations. These properties of magnetic degeneracy points can be practically important for control and readout of spin-based quantum bits.

DOI: 10.1103/PhysRevB.101.245409

I. INTRODUCTION

Nuclear and electron spins are ubiquitous constituents in condensed-matter physics. Already a few interacting quantum spins exhibit a rich variety of phenomena in rather different settings such as molecular magnets [1–3], magnetic adatoms [4,5], or spin-based quantum bits [6,7], to name a few. When studied in the three-dimensional parameter space defined by an external magnetic field, all these quantum magnets possess an intrinsic geometrical and topological structure, characterized by concepts [8,9] such as the Berry phase, the Berry curvature, and the Chern number. This geometrical structure plays an important role in coherent dynamics [10] as well as in decoherence effects [11], providing a strong motivation for exploration.

In many cases, topological considerations entail robust phenomena, governed by some global properties, insensitive to microscopic details. The quantized Hall conductance arising in the quantum Hall effect [12,13] is a prime example. In this work, we address another robust phenomenon [14,15] rooted in topology, which appears in interacting spin systems subject to a magnetic field, the emergence of ground-state degeneracies at certain magnetic fields. In this case, a topological invariant (an appropriately defined global Chern number, to be referred here as the total topological charge) predicts the existence and global properties of ground-state *magnetic degeneracy points* [2,3,8,16–18]. Most frequently, but not always, these degeneracy points are Weyl points [18], similar to linearly dispersing band-touching points in the band structure of Weyl semimetals [19], and also appearing in various physical contexts [20–22]. The precise relation of the total topological charge, the magnetic degeneracy points, and the topological charge of these points is explained in the context of molecular magnets and spin-orbit-coupled double quantum dots in Refs. [3,18], respectively.

Before introducing the specific setup and its magnetic degeneracies we will consider in this work, we briefly review the related geometric and topological concepts [8,23,24]. The Hamiltonian of a spin system $H(\boldsymbol{B})$ depends on the external magnetic field vector $\boldsymbol{B}$, defining a three-dimensional parameter space. We study such a system from the viewpoint of the ground-state manifold $|\Psi_0(\boldsymbol{B})\rangle$. The topological quantities we describe here are related to the Berry phase $\gamma(\mathcal{C})$, the geometric phase which is acquired by the ground state when we adiabatically deform the Hamiltonian in a closed path $\mathcal{C}$ of the parameter space:

$$\gamma(\mathcal{C}) = \oint_C \mathcal{A}\cdot d\boldsymbol{B} = \iint_S \mathcal{B}\cdot d\boldsymbol{S}. \tag{1}$$

Here, $\mathcal{A}(\boldsymbol{B}) = \langle\Psi_0(\boldsymbol{B})|\,\nabla_{\boldsymbol{B}}\,|\Psi_0(\boldsymbol{B})\rangle$ is the Berry connection. The second equality in Eq. (1), featuring the Berry curvature $\mathcal{B}(\boldsymbol{B}) = \nabla_{\boldsymbol{B}}\times\mathcal{A}(\boldsymbol{B})$, holds whenever Stokes' theorem can be applied to the open surface S whose boundary is the path $\mathcal{C}$. The relation between the Berry connection and the Berry curvature is similar to that of the magnetic vector potential and the magnetic field. Note that the Berry curvature can be measured experimentally [17]. The integral of the Berry curvature for a surface of the parameter space is analogous to the magnetic flux through a surface in real space. However,

*palyi@mail.bme.hu

TABLE I. Zoo of geometrical patterns and topological charge density patterns of magnetic ground-state degeneracies of a spin-orbit-coupled two-spin system. Classification is based on the eigenpatterns of the 3×3 real matrix $\hat{\boldsymbol{M}}$ with positive determinant [see Eq. (6)]. In the second column, we display the algebraic and geometrical multiplicities of positive eigenvalues. Each eigenpattern implies a geometrical pattern of the magnetic degeneracy points, which in turn implies a topological charge density pattern. The fifth column schematically shows the geometrical pattern of degeneracy points, and the topological charge of each geometrical element: +2 (orange), +1 (red), 0 (black), −1 (blue). In row (VII), the Jordan normal form may have negative or complex eigenvalues ("n/c"), and if there is only a single negative eigenvalue, then the superdiagonal element of its Jordan block can be either 0 or 1. The last column shows the stability codimension of the eigenpatterns, i.e., the number of linearly independent constraints for a small perturbation not to break the pattern.

Eigenpattern label	Multiplicities of eigenvalues	Geometric pattern	Topological charge distribution	Degeneracy points	Jordan normal form	Stability codimension
(I)	(1/1,1/1,1/1)	Six points	$4 \times (+1), 2 \times (-1)$	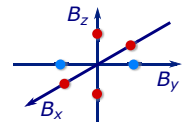	$\begin{pmatrix} a & 0 & 0 \\ 0 & b & 0 \\ 0 & 0 & c \end{pmatrix}$	0 (stable)
(II)	(2/2,1/1)	Two points, loop	$2 \times (+1), 0$	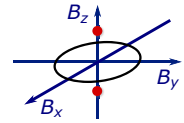	$\begin{pmatrix} a & 0 & 0 \\ 0 & a & 0 \\ 0 & 0 & b \end{pmatrix}$	3
(III)	(2/1,1/1)	Four points	$2 \times (+1), 2 \times 0$	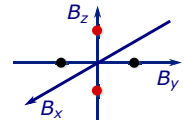	$\begin{pmatrix} a & 1 & 0 \\ 0 & a & 0 \\ 0 & 0 & b \end{pmatrix}$	1 (almost stable)
(IV)	(3/3)	Closed surface	2 (surface charge)	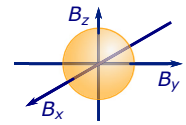	$\begin{pmatrix} a & 0 & 0 \\ 0 & a & 0 \\ 0 & 0 & a \end{pmatrix}$	8
(V)	(3/2)	Loop	2 (line charge)	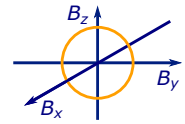	$\begin{pmatrix} a & 1 & 0 \\ 0 & a & 0 \\ 0 & 0 & a \end{pmatrix}$	4
(VI)	(3/1)	Two points	$2 \times (+1)$	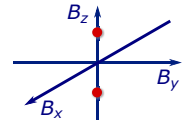	$\begin{pmatrix} a & 1 & 0 \\ 0 & a & 1 \\ 0 & 0 & a \end{pmatrix}$	2
(VII)	(1/1)	Two points	$2 \times (+1)$	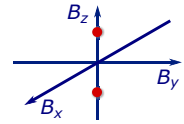	$\begin{pmatrix} a & 0 & 0 \\ 0 & \text{n/c} & 0/1 \\ 0 & 0 & \text{n/c} \end{pmatrix}$	0 (stable)

for closed surfaces, the Berry flux can be nonzero, in contrast to the magnetic flux. The Berry flux through a closed surface S in the parameter space is the Chern number associated to that surface:

$$\mathcal{Q}(S) = \frac{1}{2\pi} \oint_S \mathcal{B} \cdot d\boldsymbol{S}, \tag{2}$$

and this is an integer. The sources of this nonzero flux are the ground-state degeneracies, the points in the parameter space where the Berry curvature diverge. Hence, a topological charge is attributed to each isolated degeneracy point, whose value if the Chern number of a closed surface that encloses that degeneracy point but no other degeneracy points. The total topological charge of such a system is the Chern number of a closed surface that encloses all degeneracy points; this is equal to the sum of the topological charges of the degeneracy points.

Even though a nonzero total topological charge guarantees the existence of magnetic degeneracy points, its value does not provide a definite answer to the following questions. (i) What is the geometrical pattern (isolated points, lines, surfaces, or their combinations) drawn by the magnetic degeneracy points in the three-dimensional magnetic parameter space? (ii) How is the topological charge carried by the magnetic degeneracy points distributed among the points? (iii) Are different geometrical patterns and topological charge distributions stable against small perturbations of the system's Hamiltonian? These are nontrivial questions, and answering them probably requires extensive numerical investigations, in general.

Here, we address questions (i), (ii), and (iii) for a specific, experimentally relevant setup, a spin-orbit-coupled interacting two-spin system [18,25–31], and obtain exact results. We provide a full classification of geometrical patterns (and corresponding topological charge density patterns) of

TABLE II. Zoo of geometrical patterns and topological charge-density patterns if the g tensors have opposite signs. Notation and the structure of the table follow that in Table I. The label "neg" refers to a negative eigenvalue. In row (XI), the Jordan normal form may have negative or complex eigenvalues ("n/c"). If two or three negative eigenvalues coincide, then the superdiagonal elements of the corresponding Jordan block can be either 0 or 1.

Eigenpattern label	Description	Geometric pattern	Topological charge distribution	Degeneracy points	Jordan normal form	Stability codimension
(VIII)	(1/1,1/1)	Four points	$2\times(+1), 2\times(-1)$	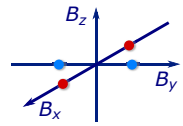	$\begin{pmatrix} a & 0 & 0 \\ 0 & b & 0 \\ 0 & 0 & \text{neg} \end{pmatrix}$	0 (stable)
(IX)	(2/2)	Loop	0	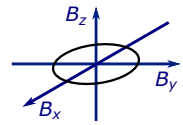	$\begin{pmatrix} a & 0 & 0 \\ 0 & a & 0 \\ 0 & 0 & \text{neg} \end{pmatrix}$	3
(X)	(2/1)	Two points	2×0	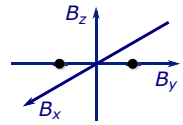	$\begin{pmatrix} a & 1 & 0 \\ 0 & a & 0 \\ 0 & 0 & \text{neg} \end{pmatrix}$	1 (almost stable)
(XI)	(-)	No points	no charge	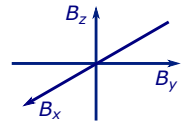	$\begin{pmatrix} \text{n/c} & 0/1 & 0 \\ 0 & \text{n/c} & 0/1 \\ 0 & 0 & \text{neg} \end{pmatrix}$	0 (stable)

the ground-state magnetic degeneracy points of this setup; this "zoo" of patterns is introduced in Tables I and II. As revealed in Tables I and II, the degeneracy points can be isolated, as in the electronic dispersion relation of a Weyl semimetal [19,32], or they can form lines or surfaces, as in nodal-loop [33] or nodal-surface [34] semimetals. In our spin-orbit-coupled interacting two-spin problem, finding the degeneracy points is reduced to the eigenvalue problem of a 3×3 nonsymmetric real matrix, and hence our analysis inherits key features of different physics subdisciplines, such as bifurcation theory [35] and non-Hermitian wave mechanics [36,37], where similar eigenvalue problems play important roles. Beyond fundamental interest, the properties of magnetic degeneracy points are in fact practically important for control and readout of spin-based quantum bits; two-electron singlet-triplet degeneracy points, e.g., are often exploited for spin initialization, control, and readout [6,30,31,38–40].

We consider a system of two interacting localized electrons, subject to spin-orbit interaction, and assume that they are placed in a homogeneous magnetic (Zeeman) field [Fig. 1(a)]. This system can be described by a 4×4 Hamiltonian matrix [18]

$$H = H_{\rm Z} + H_{\rm int}, \tag{3a}$$

$$H_{\rm Z} = \mu_{\rm B}\boldsymbol{B}\cdot(\hat{\boldsymbol{g}}_{\rm L}\boldsymbol{S}_{\rm L} + \hat{\boldsymbol{g}}_{\rm R}\boldsymbol{S}_{\rm R}), \tag{3b}$$

$$H_{\rm int} = J\boldsymbol{S}_{\rm L}\cdot\hat{\boldsymbol{R}}\boldsymbol{S}_{\rm R}. \tag{3c}$$

Here, $H_{\rm Z}$ is the Zeeman interaction with the external homogeneous magnetic field $\boldsymbol{B}$, $H_{\rm int}$ is the spin-orbit-affected exchange interaction between the two electrons, $\mu_{\rm B}$ is the Bohr magneton, $\hat{\boldsymbol{g}}_{\rm L}$ and $\hat{\boldsymbol{g}}_{\rm R}$ are the real-valued, spin-orbit-affected g tensors of the two electrons, $\boldsymbol{S}_{\rm L}$ and $\boldsymbol{S}_{\rm R}$ are the spin vector operators represented by $\frac{1}{2}$ times the spin-$\frac{1}{2}$ Pauli matrices, $J>0$ is the strength of the exchange interaction, and $\hat{\boldsymbol{R}}$ is a real, 3×3 special orthogonal matrix accounting for the spin-orbit interaction in the exchange term.

The exchange interaction term $H_{\rm int}$ we use in Eq. (3c) was derived from a two-site Hubbard model at zero magnetic field, where spin-orbit interaction appears as a spin-dependent tunneling term [18,41] between the two sites. The

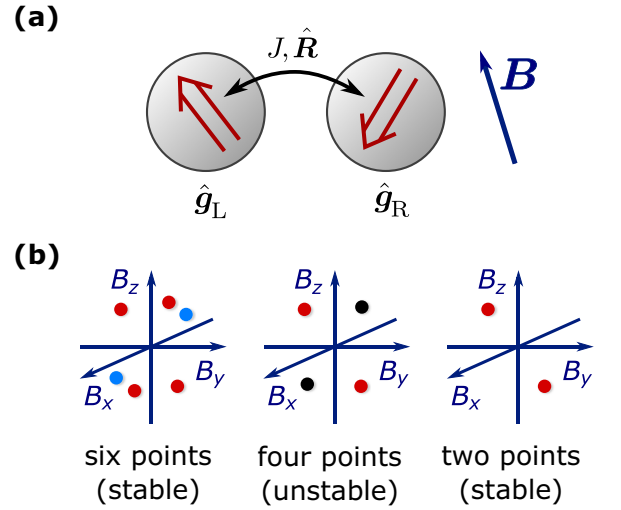

FIG. 1. Magnetic degeneracy points of two interacting spin-$\frac{1}{2}$ electrons. (a) Exchange interaction between the spins is described by its strength J and a rotation $\hat{\boldsymbol{R}}$. External magnetic field $\boldsymbol{B}$ couples to the spins through the g tensors. (b) Geometry and topological charge distribution of magnetic degeneracy points for $\det\hat{\boldsymbol{g}}_{\rm L}, \det\hat{\boldsymbol{g}}_{\rm R} > 0$. Colors indicate topological charge: $+1$ (red), -1 (blue), 0 (black). Six-point and two-point patterns are stable, and the generic transition between these patterns is when two oppositely charged pairs meet and their charges annihilate each other (four points).

two-electron sector of this Hubbard model is a 6×6 matrix, which can be projected to the 4×4 exchange Hamiltonian [18,25] above by eliminating the states with doubly occupied sites via quasidegenerate perturbation theory. It is tempting to associate a spatial direction to the spin-dependent tunneling, e.g., the direction of the rotation axis of $\hat{\boldsymbol{R}}$. Here, we avoid that because that spatial direction is gauge dependent, that is, it depends on the choice of the Kramers-pair single-particle basis states, as discussed below.

In the Zeeman Hamiltonian of Eq. (3b), the g tensors are arbitrary real matrices, which are not necessarily symmetric. One way to think about their effect is that the spins feel potentially different effective magnetic fields $\boldsymbol{B}_{\mathrm{L/R,eff}} = \hat{\boldsymbol{g}}^{\mathrm{T}}_{\mathrm{L/R}}\boldsymbol{B}$ instead of the external magnetic field. For concreteness, let us first focus on the case when the determinants of both g tensors are positive, $\det(\hat{\boldsymbol{g}}_{\mathrm{L}})$, $\det(\hat{\boldsymbol{g}}_{\mathrm{R}}) > 0$. The elements of the three 3×3 matrices $\hat{\boldsymbol{g}}_L$, $\hat{\boldsymbol{g}}_R$, and $\hat{\boldsymbol{R}}$ are determined by microscopic details (spin-orbit interaction, confinement potential, choice of basis, etc.), but here we treat them as possibly independent phenomenological parameters.

In our topological considerations, we distinguish the three Cartesian magnetic-field components B_x, B_y, B_z in the Hamiltonian as "primary" parameters, and refer to further parameters as "secondary" ones. In this nomenclature, secondary parameters are fixed, while primary parameters are thought of as external parameters, varied continuously. At certain points within the space of primary parameters, the ground state of H becomes degenerate. We refer to these points as *magnetic degeneracy points*.

We have studied this two-spin system in detail in our recent work [18]. There, we have shown that in the case $\det(\hat{\boldsymbol{g}}_{\mathrm{L}})$, $\det(\hat{\boldsymbol{g}}_{\mathrm{R}}) > 0$, (i) topological considerations guarantee the existence of ground-state magnetic degeneracy points (often, but not always, magnetic Weyl points), irrespective of microscopic details of the Hamiltonian, (ii) the degeneracy points carry topological charge, and the total topological charge carried by all degeneracy points of the three-dimensional magnetic-field parameter space sums up to $+2$. By numerical work and intuitive considerations, we have demonstrated four different geometrical patterns formed by the magnetic degeneracy points, and the corresponding topological charge distributions: (a) A sphere, carrying a surface topological charge of $+2$. This is the case without spin-orbit interaction, when the g tensors are isotropic and the exchange interaction is of antiferromagnetic Heisenberg type ($J\boldsymbol{S}_{\mathrm{L}} \cdot \boldsymbol{S}_{\mathrm{R}}$). This case also provides an example where the magnetic degeneracy points are not Weyl points. (b) Two isolated (Weyl) points, each carrying charge $+1$. (c) Six isolated (Weyl) points, four of them carrying charge $+1$, two of them carrying charge -1. (D) Four isolated points, two of them carrying charge $+1$, the other two carrying no charge. [See Fig. 1(b) of this work or Fig. 4(a) of Ref. [18]].

We note that we use the term Weyl point to label an isolated degeneracy point that possesses all of the following properties: (1) the energy splitting in its vicinity increases linearly with small deviation in the parameter space, in all directions, (2) the degeneracy is twofold, and (3) the absolute value of its topological charge is one [which, by the way, follows from points (1) and (2)]. Accordingly, we did not label the charge-neutral degeneracy points in case (d) above as Weyl-points, since they violate both points (1) and (3). In the condensed-matter literature, band degeneracy points not showing at least one of the above three properties are sometimes called multi-Weyl points [32,42–44], but we do not use this terminology here.

Going beyond our earlier numerical study, here we develop an analytical approach, which allows for a complete classification of the geometrical and topological structure of magnetic degeneracy points. For this analysis, it is important to distinguish three cases defined by the three possible values of the total topological charge $\mathcal{Q}$. This charge is the sum of the g-tensor signs, i.e., $\mathcal{Q} = \mathrm{sgn}(\det \hat{\boldsymbol{g}}_{\mathrm{L}}) + \mathrm{sgn}(\det \hat{\boldsymbol{g}}_{\mathrm{R}})$, and hence $\mathcal{Q} \in \{-2, 0, 2\}$. We will show that the geometrical patterns are the same in case $\mathcal{Q} = +2$ (Table I) and case $\mathcal{Q} = -2$, although the topological charges are the opposite in the two cases. Also, we will show that the geometrical patterns are distinct in the case $\mathcal{Q} = 0$ (Table II). Rephrasing this in terms of the relative sign $\mathcal{S} = \mathrm{sgn}[\det(\hat{\boldsymbol{g}}_{\mathrm{L}}) \cdot \det(\hat{\boldsymbol{g}}_{\mathrm{R}})]$, we can say that the geometrical patterns are different for the two possible values $\mathcal{S} \in \{-1, +1\}$.

For $\mathcal{S} = +1$ we obtain a sixfold classification of geometrical patterns of magnetic degeneracy points (Table I), corresponding to six different topological charge distributions (i.e., two more beyond the ones identified in Ref. [18]), and further four possible classes are identified for $\mathcal{S} = -1$. These form altogether *10 geometrical classes*. Note that geometrical patterns of magnetic degeneracy points for a different class of Hamiltonians were studied recently in Ref. [45].

Furthermore, we use our approach to characterize the stability of these patterns against small perturbations of the Hamiltonian [see Fig. 1(b)]: we find two stable and one almost stable charge configurations both for $\mathcal{S} = +1$ and for $\mathcal{S} = -1$, the almost stable magnetic configuration forming a generic boundary between stable configurations, similar to bifurcations in the theory of dynamical systems [35].

The rest of the paper is structured as follows. In Sec. II, we derive a classification of the geometrical patterns and topological charge density patterns of magnetic degeneracy points for the case $\mathcal{S} = +1$, with the main results summarized in Table I. In Sec. III, we analyze the stability of each of these patterns against perturbations of the Hamiltonian. In Sec. IV, we extend the results to case $\mathcal{S} = -1$, and provide our conclusions in Sec. V.

II. CLASSIFICATIONS OF DEGENERACY POINTS

A. Mapping the degeneracy problem to the eigenproblem of a nonsymmetric matrix

Given the Hamiltonian (3), it is not obvious how to analyze the geometrical patterns formed by the magnetic degeneracy points. One could, in principle, find the eigenvalues of the 4×4 Hamiltonian (3) analytically, and investigate, in a very large dimensional parameter space, the conditions under which ground-state degeneracies occur. Numerical diagonalization and numerical search for the magnetic degeneracy points is also an option, but this requires a lot of computational effort and is most likely incomplete [18].

Fortunately, for the specific Hamiltonian (3), a simple observation allows for a fully analytical treatment of the

problem. As a first step, we introduce a local spin transformation $\mathcal{U}_1 = \mathbb{1} \otimes U_R(\hat{\boldsymbol{R}})$ on the right spin to eliminate the rotation $\hat{\boldsymbol{R}}$ appearing in the exchange term. If $\hat{\boldsymbol{R}}$ is a rotation around the unit vector $\boldsymbol{n}$ with angle α, then the corresponding unitary transformation [46] is

$$U_R(\hat{\boldsymbol{R}}) = \exp(-i\alpha\, \boldsymbol{n} \cdot \boldsymbol{S}_R). \tag{4}$$

This transformation renders the exchange interaction isotropic. The transformed Hamiltonian $H' = \mathcal{U}_1 H \mathcal{U}_1^\dagger$ now reads as

$$H' = \mu_B(\boldsymbol{B}'_{L,\mathrm{eff}} \cdot \boldsymbol{S}_L + \boldsymbol{B}'_{R,\mathrm{eff}} \cdot \boldsymbol{S}_R) + J\boldsymbol{S}_L \cdot \boldsymbol{S}_R, \tag{5}$$

where the effective magnetic fields felt by the left and right spins read as $\boldsymbol{B}'_{L,\mathrm{eff}} = \hat{\boldsymbol{g}}_L^{\mathrm{T}}\boldsymbol{B}$ and $\boldsymbol{B}'_{R,\mathrm{eff}} = \hat{\boldsymbol{R}}\hat{\boldsymbol{g}}_R^{\mathrm{T}}\boldsymbol{B}$. The right effective magnetic field is rotated with $\hat{\boldsymbol{R}}$ in the new basis. Note that throughout this paper, the spin operators $\boldsymbol{S}_{L/R}$ are defined as $\frac{1}{2}$ times the vectors of Pauli matrices.

Already from Eq. (5) it is apparent that if the effective magnetic fields are parallel, then we can take their common direction as the spin quantization axis (z), and in that frame, the z component of the total spin is conserved. This has the consequence that as B is increased from zero to infinity along that specific direction, a ground-state level *crossing* arises at a specific value of B. See Appendix C for details.

The above observations imply that for finding the magnetic degeneracy points, we do not have to solve the eigenvalue problem of the 4×4 Hamiltonian, but it is instead sufficient to find the magnetic-field directions for which $\boldsymbol{B}'_{L,\mathrm{eff}} \parallel \boldsymbol{B}'_{R,\mathrm{eff}}$. An elementary proof shows that this condition is satisfied, if and only if $\boldsymbol{B}$ is a (left) eigenvector of the 3×3 matrix

$$\hat{\boldsymbol{M}} = \hat{\boldsymbol{g}}_L \hat{\boldsymbol{R}} \hat{\boldsymbol{g}}_R^{-1}. \tag{6}$$

A magnetic degeneracy point is found in this direction if the eigenvector belongs to a positive eigenvalue of $\hat{\boldsymbol{M}}$. Note that $\hat{\boldsymbol{M}}$ is real, but in general it is not symmetric. Hence, in conclusion, we have mapped the problem of finding the magnetic degeneracy points to the eigenproblem of a 3×3 nonsymmetric real matrix.

B. Eigenpattern of the matrix $\hat{\boldsymbol{M}}$ and the geometrical pattern of the magnetic degeneracy points

As we now show, the structure of the eigenvalues and eigenvectors of the matrix $\hat{\boldsymbol{M}}$ implies the geometrical pattern of the magnetic degeneracy points. For concreteness, throughout the rest of Sec. II and also in Sec. III, we focus on the case where the determinants of both g tensors are positive, $\det(\hat{\boldsymbol{g}}_L), \det(\hat{\boldsymbol{g}}_R) > 0$, that is, $\mathcal{S} = +1$ and $\mathcal{Q} = +2$. The results obtained trivially generalize to the case $\det(\hat{\boldsymbol{g}}_L), \det(\hat{\boldsymbol{g}}_R) < 0$ ($\mathcal{S} = +1$, $\mathcal{Q} = -2$), with the only modification that the total topological charge of the ground-state magnetic degeneracy points has opposite sign in the latter case, and correspondingly, all topological charges in the discussions below are reversed.

The case $\mathcal{S} = -1$ ($\mathcal{Q} = 0$) is, however, quite different. Then, the total topological charge of the magnetic degeneracy points adds up to zero, implying a completely different structure of the eigenproblem of $\hat{\boldsymbol{M}}$, and thereby different geometrical patterns and topological charge distributions. This case will be discussed in Sec. IV.

For $\det(\hat{\boldsymbol{g}}_L), \det(\hat{\boldsymbol{g}}_R) > 0$, the 3×3 matrix $\hat{\boldsymbol{M}}$ is real but nonsymmetric in general, and it has a positive determinant because the g tensors have positive determinants, and $\det \hat{\boldsymbol{R}} = 1$. To see the possible geometries of the magnetic degeneracy points, we first have to identify qualitatively different solutions of the eigenproblem of $\hat{\boldsymbol{M}}$.

As we show below, for $\det(\hat{\boldsymbol{g}}_L), \det(\hat{\boldsymbol{g}}_R) > 0$ there are seven different cases, labeled from (I) to (VII) in Table I, that are classified by the number of positive eigenvalues, and their algebraic and geometric multiplicities. (For a brief summary of the relevant concepts and relations of linear algebra, see Appendix A). We call these cases the *eigenpatterns* of the matrix $\hat{\boldsymbol{M}}$, and will use, e.g., $\mathrm{ep}(\hat{\boldsymbol{M}}) = (\mathrm{IV})$, to denote that the eigenpattern of $\hat{\boldsymbol{M}}$ is (IV).

For $\mathrm{ep}(\hat{\boldsymbol{M}}) = (\mathrm{I})$, the matrix $\hat{\boldsymbol{M}}$ has three different positive eigenvalues, a, b, and c. The algebraic and geometric multiplicities are all 1, as denoted in the second column of Table I. Let us denote the normalized left eigenvectors with $\boldsymbol{v}_a$, $\boldsymbol{v}_b$, and $\boldsymbol{v}_c$. Then, there are six magnetic degeneracy points, one time-reversed pair associated to each eigenvector $\boldsymbol{v}_\alpha$, appearing if the magnetic field is aligned or antialigned with those eigenvectors. The locations of the degeneracy points in the original magnetic-field parameter space are

$$\boldsymbol{B}_{\alpha,\pm} = \pm B_\alpha \cdot \boldsymbol{v}_\alpha \quad (\alpha \in a, b, c). \tag{7}$$

The expressions for the critical fields B_α, and their derivations are summarized in Appendix C. Topological charges of these degeneracy points are discussed below.

Two further eigenpatterns arise when $\hat{\boldsymbol{M}}$ has two different positive eigenvalues, a and b [see Table I, rows (II) and (III)]. In these cases, one of these eigenvalues, say a, must have an algebraic multiplicity of 2. (Otherwise, either $\hat{\boldsymbol{M}}$ would have a third, negative eigenvalue, which is forbidden by the fact the $\hat{\boldsymbol{M}}$ has positive determinant, or it would have a third, complex eigenvalue, which is forbidden by the fact that complex eigenvalues come in complex-conjugate pairs.) Then, a can have a geometric multiplicity of 2, yielding case (II) in Table I, or a geometric multiplicity of 1, yielding case (III). In case (II), the magnetic degeneracy points are arranged at two isolated points along the line of $\boldsymbol{v}_b$, at $\boldsymbol{B}_{b,\pm} = \pm B_b \cdot \boldsymbol{v}_b$, and along an ellipse in the plane spanned by the two remaining eigenvectors $\boldsymbol{v}_{a_1}$ and $\boldsymbol{v}_{a_2}$. See Appendix D for details. In case (III), the magnetic degeneracy points are arranged in four isolated points, similarly at $\boldsymbol{B}_{a,\pm} = \pm B_a \cdot \boldsymbol{v}_a$ and $\boldsymbol{B}_{b,\pm} = \pm B_b \cdot \boldsymbol{v}_b$.

Four further eigenpatterns appear when $\hat{\boldsymbol{M}}$ has a single positive eigenvalue $a > 0$ [see rows (IV)–(VII) of Table I]. These eigenvalues can have an algebraic multiplicity of 3, and a geometric multiplicity of 3, yielding case (IV), where the magnetic degeneracy points form a closed surface, an ellipsoid. The simplest example is the case without spin-orbit interaction, where the g tensors and $\hat{\boldsymbol{R}}$ are all proportional to the unit matrix, and the magnetic degeneracy points form a sphere. Alternatively, a can have an algebraic multiplicity of 3, and a geometric multiplicity of 2, yielding case (V), where the magnetic degeneracy points form a closed loop, an ellipse. Yet another alternative is that a has a geometric multiplicity of 1, yielding case (VI), with two isolated magnetic degeneracy points.

Finally, it can also have an algebraic multiplicity of 1, and consequently a geometric multiplicity of 1, denoted as case (VII), yielding two isolated magnetic degeneracy points. This sevenfold classification of the relevant solutions of the eigenvalue problem implies a sixfold classification of the qualitatively different geometrical patterns of the magnetic degeneracy points since the eigenpatterns (VI) and (VII) yield the same geometry.

C. Topological charge-density patterns

We know that the magnetic degeneracy points can also carry a topological charge [18], and for our Hamiltonian with fixed secondary parameters, the total charge is $\mathcal{Q} = +2$. In principle, it could happen that two different Hamiltonians yield the same geometry of degeneracy points, but the charge is distributed differently among the elements. For example, in case (II), the ellipse-shaped loop could be neutral and the isolated points could carry charge $+1$ each, or the points could be neutral and the ellipse could carry charge $+2$. As we show in Appendix E, in our model, the topological charge density is uniquely determined by the geometrical pattern; in the example above, the points are charged and the loop is neutral. The topological charge density patterns are listed in the fourth column and sketched in the fifth column of Table I.

III. STABILITY ANALYSIS OF EIGENPATTERNS AND CORRESPONDING GEOMETRICAL PATTERNS

In Ref. [18], we have studied random Hamiltonians for this spin-orbit-coupled two-spin model numerically, and among those random Hamiltonians, we have identified only two of the above six different geometrical patterns, the "six-points" pattern and the "two-points" pattern. Why do not we find representatives of the other four geometrical patterns in a random ensemble of Hamiltonians? As we argue below, each eigenpattern can be characterized by a "degree of stability" or "codimension," denoted by d, which is a non-negative integer, familiar from the codimension property of bifurcations [35]: if $d = 0$, then the eigenpattern is stable, if $d > 0$, then the eigenpattern is unstable, and an increasing d is interpreted as decreasing stability: the larger d, the more parameters of H need to be tuned to observe the given eigenpattern and the corresponding magnetic pattern. We will show that the six-points pattern and the two-points pattern are the only stable patterns, providing an explanation for our earlier numerical findings.

We define stability via sensitivity to small random perturbations. Consider the Hamiltonian H of Eq. (3) with fixed secondary parameters, which specifies the matrix $\hat{\boldsymbol{M}}$, which in turn has a specific eigenpattern. If we slightly modify the secondary parameters, and thereby add an infinitesimal perturbation $H \to H' = H + \delta H$, then the eigenpattern of H' may be the same as that of H, or it may be different. (Note that throughout this section, the prime in H' and related quantities refers to a perturbed instance of the quantity, unlike in other sections.) If the eigenpattern of H' is the same as that of H for any infinitesimal perturbation δH, then we call the eigenpattern of H stable. Otherwise, we call it unstable.

Instead of considering H directly, we address the question of eigenpattern stability by regarding the matrix $\hat{\boldsymbol{M}}$ as the element of a nine-dimensional vector space.[1] The infinitesimal perturbations $\delta\hat{\boldsymbol{M}}$ span a nine-dimensional vector space, too; we denote this vector space by W. The question of eigenpattern stability can then be phrased as follows: for a given $\hat{\boldsymbol{M}}$, what is the dimension of the subspace $W_\mathrm{s} \leqslant W$ spanned by the infinitesimal perturbations $\delta\hat{\boldsymbol{M}}$ that preserve the eigenpattern of $\hat{\boldsymbol{M}}$ under $\hat{\boldsymbol{M}} \to \hat{\boldsymbol{M}}' = \hat{\boldsymbol{M}} + \delta\hat{\boldsymbol{M}}$? If $\dim(W_\mathrm{s}) = 9$, then the eigenpattern is preserved for an arbitrary infinitesimal perturbation, i.e., the eigenpattern of $\hat{\boldsymbol{M}}$ is stable. Otherwise, it is unstable, and the degree of stability can be characterized by the codimension of the stable subspace W_s, which is $d \equiv 9 - \dim(W_\mathrm{s})$, with $d = 0$ denoting the stable case and increasing d signaling increasing instability.

We now outline a method to calculate d for a given $\hat{\boldsymbol{M}}$. This is based on the Jordan decomposition of $\hat{\boldsymbol{M}}$ (see Appendix A),

$$\hat{\boldsymbol{M}} = \hat{\boldsymbol{P}}\hat{\boldsymbol{J}}\hat{\boldsymbol{P}}^{-1}, \tag{8}$$

with $\hat{\boldsymbol{J}}$ being the Jordan normal form of $\hat{\boldsymbol{M}}$, and $\hat{\boldsymbol{P}}$ a similarity transformation. Let us choose $\mathrm{ep}(\hat{\boldsymbol{M}}) = (\mathrm{V})$ as our example, so its Jordan normal form reads as

$$\hat{\boldsymbol{J}} = \begin{pmatrix} \lambda & 1 & 0 \\ 0 & \lambda & 0 \\ 0 & 0 & \lambda \end{pmatrix}. \tag{9}$$

The matrix $\hat{\boldsymbol{M}}$ has thus one eigenvalue with an algebraic multiplicity of 3 but only two linearly independent corresponding eigenvectors. Recall that this eigenpattern implies that the magnetic degeneracy points are located on an ellipse.

We first characterize those perturbations of $\hat{\boldsymbol{M}}$ which preserve this eigenpattern, that is, preserve the structure of the Jordan form. For these, the Jordan form of the deformed matrix $\hat{\boldsymbol{M}}'$ must read as

$$\hat{\boldsymbol{J}}' = \hat{\boldsymbol{J}} + \delta\hat{\boldsymbol{J}} = \hat{\boldsymbol{J}} + \begin{pmatrix} \nu & 0 & 0 \\ 0 & \nu & 0 \\ 0 & 0 & \nu \end{pmatrix}, \tag{10}$$

with an infinitesimal ν. Since the only constraint on the perturbation is that the eigenpattern (that is, the Jordan normal form) should be preserved, an arbitrary infinitesimal change is allowed in the similarity transformation $\hat{\boldsymbol{P}}$,

$$\hat{\boldsymbol{P}}' = \hat{\boldsymbol{P}}(\mathbb{1} + \delta\hat{\boldsymbol{B}}) \tag{11}$$

with an infinitesimal term

$$\delta\hat{\boldsymbol{B}} = \begin{pmatrix} b_{11} & b_{12} & b_{13} \\ b_{21} & b_{22} & b_{23} \\ b_{31} & b_{32} & b_{33} \end{pmatrix}. \tag{12}$$

Now we have parametrized, using 10 infinitesimal parameters (the b_{ij}'s and ν), all matrices that are infinitesimally close to $\hat{\boldsymbol{M}}$ and have the same eigenpattern as $\hat{\boldsymbol{M}}$; in fact, we have overparametrized $\hat{\boldsymbol{M}}$. We can express the shift of the matrix $\hat{\boldsymbol{M}}$

[1] We can modify all elements of $\hat{\boldsymbol{M}}$ by changing some parameters of the original Hamiltonian.

up to linear order in these infinitesimal parameters as

$$\delta\hat{\boldsymbol{M}} = \hat{\boldsymbol{M}}' - \hat{\boldsymbol{M}} = \hat{\boldsymbol{P}}'\hat{\boldsymbol{J}}'\hat{\boldsymbol{P}}'^{-1} - \hat{\boldsymbol{P}}\hat{\boldsymbol{J}}\hat{\boldsymbol{P}}^{-1}$$
$$= \hat{\boldsymbol{P}}([\delta\hat{\boldsymbol{B}}, \hat{\boldsymbol{J}}] + \delta\hat{\boldsymbol{J}})\hat{\boldsymbol{P}}^{-1} \equiv \hat{\boldsymbol{P}}\,\delta\hat{\tilde{\boldsymbol{M}}}\,\hat{\boldsymbol{P}}^{-1}. \quad (13)$$

Not all our infinitesimal parameters lead, however, to independent deformations of $\hat{\boldsymbol{M}}$. To determine *independent* deformations, we note that $\delta\hat{\tilde{\boldsymbol{M}}} = \delta\hat{\tilde{\boldsymbol{M}}}(\{b_{ij}\}, \nu)$ is a homogeneous linear function of the infinitesimal parameters, that is,

$$\delta\hat{\tilde{\boldsymbol{M}}}_{ij} = \sum_{\gamma=1}^{10} C_{ij,\gamma}\epsilon_\gamma \quad (i, j = 1, 2, 3), \quad (14)$$

where $(\{\epsilon_\gamma\}) = (\{b_{ij}\}, \nu)$ is the 10-tuple of the infinitesimal parameters, and the coefficients of the linear relation are arranged in the 9×10 matrix C. This linear relation (14) together with the similarity transformation (13) implies that the dimension of the image $\delta\hat{\boldsymbol{M}}$ of the 10-dimensional vector space of the infinitesimal parameters is simply rank(C). The dimension of the stable subspace of perturbations is therefore $\dim(W_\mathrm{s}) = \mathrm{rank}(C)$.

A straightforward calculation shows that in this specific case, $\dim(W_\mathrm{s}) = \mathrm{rank}(C) = 5$. Correspondingly, the stability codimension is $d = 9 - \dim(W_\mathrm{s}) = 4$ for eigenpattern (V) (cf. Table I). We therefore conclude that the eigenpattern (V) has a rather high codimension d, and is therefore quite unstable, i.e., it is difficult to observe it in nature.

The stability of each of the seven eigenpatterns in Table I can be characterized by calculating the corresponding codimension d in a similar way. The results are shown in the seventh column of Table I. The most important result is that the stability codimension of eigenpatterns (I) and (VII) is zero, hence, these are the stable eigenpatterns and, consequently, these provide two geometrical patterns of the magnetic degeneracy points: the two-points configuration (VII), and the six-points configuration (I). This result explains and corroborates our earlier numerical finding [18], where only these two geometrical patterns were found by studying randomized Hamiltonians.

Note that the six-points geometrical pattern is always stable; however, the two-points configuration can also be unstable, when the eigenpattern (VI) is realized. In fact, when the Hamiltonian belonging to eigenpattern (VI) is subject to an arbitrary infinitesimal perturbation $\delta\hat{\boldsymbol{M}}$, then it might (i) preserve its eigenpattern (if $\delta\hat{\boldsymbol{M}} \in W_\mathrm{s}$), or (ii) change its eigenpattern to (VII), or (iii) change its eigenpattern to (I), i.e., the two degeneracy points can split into three pairs of Weyl points, or (iv) change its eigenpattern to (III), i.e., the two degeneracy points split into a Weyl and a neutral point pair.

It is also remarkable that the textbook case of a spherical surface geometry of the magnetic degeneracy points a special case of (IV) provided by isotropic g factors and isotropic Heisenberg interaction, is the *most unstable* of all configurations: its stability codimension $d = 8$ is maximal among the seven eigenpatterns.

A further question is as follows: How do transitions between stable eigenpatterns take place upon changing the secondary parameters of the Hamiltonian? If we consider two Hamiltonians from the two different stable eigenpattern classes (I) and (VII), and continuously interpolate between them, then there must be a critical point on the way where four of the six points disappear. The answer is given by Table I, and also depicted in Fig. 1(b): the only geometric pattern with a stability codimension 1 is the "four-points" pattern, hence, this is the generic boundary between the two stable geometric patterns. To reach the remaining four patterns, further fine tuning is required.

IV. PATTERNS OF MAGNETIC DEGENERACY POINTS FOR $\mathcal{S} = -1$

Patterns of magnetic degeneracy points appearing for a negative relative sign $\mathcal{S} = -1$ of the g tensors are different from the ones discussed in the previous two sections. In this case, the total topological charge of the ground-state magnetic degeneracy points is $\mathcal{Q} = 0$. This indicates that generic Hamiltonians could exist without *any* magnetic degeneracy. Also, since Weyl points must appear in $\pm\boldsymbol{B}$ pairs, and their charge must add up to 0, we expect other generic situations with four magnetic Weyl points, two with topological charge $+1$ and two with topological charge -1.

These expectations are indeed confirmed by the eigenpattern analysis of the matrix $\hat{\boldsymbol{M}}$. The analysis follows the steps of the previous section. The matrix $\hat{\boldsymbol{M}}$ defined in Eq. (6) has a negative determinant in this case, but still the magnetic degeneracy points are associated with the positive eigenvalues of $\hat{\boldsymbol{M}}$. The negative determinant of $\hat{\boldsymbol{M}}$ implies that the combinations of algebraic and geometric multiplicities of its eigenvalues are different from the positive-determinant case in the main text. Apart from these differences, the analysis is very similar, hence we omit the details here, and summarize the results in Table II.

In this case, we find two stable eigenpatterns with codimension $d = 0$, eigenpatterns (VIII) and (XI). Pattern (XI) corresponds to the trivial case, with no magnetic degeneracy at any field, while pattern (VIII) to the case of having two positively charged and two negatively charged Weyl points. One of the important messages of Table II is that there is no other stable configuration. The almost stable eigenpattern (X) of two chargeless degeneracy points is the generic pattern, separating extended regions (VIII) and (XI) of stable configurations in parameter space. These are precisely the points at which two oppositely charged Weyl points merge and annihilate each other (see Fig. 2). The remaining eigenpattern (IX) corresponds to a loop of magnetic degeneracy points and, with codimension $d = 3$, is very unstable.

V. CONCLUSIONS

In conclusion, we have provided a full analytical description of the geometrical patterns and topological charge distribution patterns of magnetic ground-state degeneracy points in a spin-orbit-coupled two-spin system. By recognizing the special structure of the Hamiltonian, we have mapped the problem of finding the degeneracy points to the eigenproblem of a real nonsymmetric 3×3 matrix. We have found three distinct regions in the space of (secondary) parameters, according to the total topological charge in magnetic (primary) parameter space $\mathcal{Q} = \mathrm{sgn}(\det\hat{\boldsymbol{g}}_\mathrm{L}) + \mathrm{sgn}(\det\hat{\boldsymbol{g}}_\mathrm{R})$.

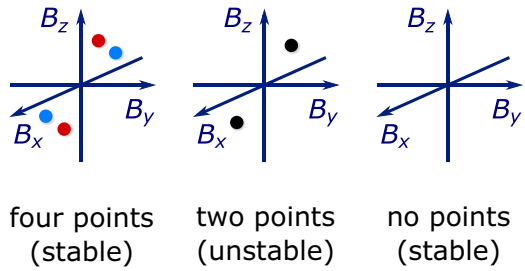

FIG. 2. Magnetic degeneracy points for two interacting spin-$\frac{1}{2}$ electrons, when the relative sign of the g tensors is negative, $\mathcal{S} = -1$. Color of each point indicates its topological charge: $+1$ (red), -1 (blue), 0 (black). Four-points and no-points patterns are stable, and the generic transition between them is that the two oppositely charged pairs meet and their charges annihilate each other (two points).

The regions $\mathcal{Q} = \pm 2$ are very similar, only the signs of the charge distributions are the opposite. In both regions, our stability analysis reveals the existence of two stable and extended (i.e., nonzero measure) regions in the secondary parameter space: in the first one, case (VII), two magnetic Weyl points carry the topological charge, while in the second one, case (I), six Weyl points carry the total charge $\mathcal{Q} = 4 \times (+1) + 2 \times (-1)$. There is *no other* geometrically stable region, meaning that other charge patterns exist only in special, fine-tuned Hamiltonians, realized for secondary parameters forming a set of zero measure. Some of these configurations can, however, be observed. For $\mathcal{Q} = +2$, the unstable configuration that is the most stable is the one with two merged Weyl points, that is, when ep($\hat{\boldsymbol{M}}$) = (III). This configuration (III) emerges at the *boundary* between the two topologically stable phases, (I) and (VII). We naturally cross this surface in case we change some of the secondary parameters of the Hamiltonian, such that we go continuously from a region with ep($\hat{\boldsymbol{M}}$) =(I) to a region with ep($\hat{\boldsymbol{M}}$) =(VII). Approaching this surface, a positively and negatively charged pair of Weyl points must approach each other, and just merge to annihilate each other. This boundary, corresponding to ep($\hat{\boldsymbol{M}}$) =(III), includes further special patterns, corresponding to further fine tuning of the parameters.

A similar picture emerges for the case $\mathcal{Q} = 0$. There, two generic, extended regions are found with no degeneracy points [ep($\hat{\boldsymbol{M}}$) = (XI)], and with four Weyl points [ep($\hat{\boldsymbol{M}}$) = (VIII)], respectively. The generic surface between them corresponds to ep($\hat{\boldsymbol{M}}$) =(X), with two neutral degeneracy points, where the two pairs of Weyl points just merged. These magnetic degeneracy patterns are shown in Fig. 2.

The linear stability of regions (I), (VII), (VIII), and (XI) is corroborated by robust topological arguments: Weyl points cannot disappear upon infinitesimal smooth deformations of the secondary parameters. Starting from these configurations, removing Weyl points or creating new degeneracy points requires fine tuning of the parameters: either positive and negative charges must move toward each other, and then annihilate at a very special point [this corresponds to the boundaries (III) and (X) discussed above], or fine tuning leads to the formation of an ellipse or an ellipsoid of degeneracy points that are not Weyl points, as their energy dispersion is flat in at least one direction. Numbers and charges of the Weyl points in regions (I), (VII), (VIII), and (XI) are constrained by the total topological charge, whereas the relative locations of these Weyl points are constrained by the fact that they always come in time-reversed pairs [18].

The classification problem studied here is readily generalized to any interacting spin system, e.g., three interacting electrons subject to spin-orbit coupling, or two interacting spins with larger spin size. Studying possible geometrical patterns of the magnetic degeneracy points, the corresponding topological charge-density patterns, the stability of these and their evolution upon continuous deformations of the Hamiltonian are interesting and challenging tasks.

A further direction for generalization is to analyze magnetic degeneracy points of higher-energy eigenstates instead of the ground state [3]. An interesting set of further problems is obtained if the spin-orbit effects are not completely arbitrary, but are subject to symmetry constraints. For example, if magnetic adatoms are placed on specific sites on a metallic surface [4,5], then the spatial symmetry of the arrangement will restrict the form of the g tensors and the exchange terms. In general, a fully numerical approach can provide insight into the questions above, but it seems difficult to efficiently generalize the analytical treatment used here to obtain exact results for a much broader set of physically motivated Hamiltonians.

Aside from opening up interesting theory questions, we hope that our work will inspire experiments as well. Weyl points in interacting spin systems have been found experimentally by transport [18] and Landau-Zener spectroscopy [1], but their topological characterization, e.g., via measurements of the Berry curvature [16,17], is yet to be done. To observe a sharp transition between different eigenpatters studied here, e.g., to observe creation and annihilation of Weyl points, the experimenter needs exquisite control over the g tensors and/or spin-spin interaction. This is given, to some extent, in spin-orbit-coupled quantum dots [47,48], but a fruitful alternative realization could be done in superconducting qubits, where synthetic qubit-qubit interaction, including antisymmetric exchange [49], can be engineered and controlled.

ACKNOWLEDGMENTS

We thank G. Pintér, P. Vrana, and H. Weng for useful discussions. This work was supported by the National Research Development and Innovation Office of Hungary within the Quantum Technology National Excellence Program (Project No. 2017-1.2.1-NKP-2017-00001), under OTKA Grants No. 124723, No. 127900, and No. 132146 by the New National Excellence Program of the Ministry of Human Capacities, by the BME-Nanotechnology FIKP grant (BME FIKP-NAT), by the QuantERA SuperTop project, and by the AndQC FetOpen project.

APPENDIX A: SURVIVAL KIT FOR THE EIGENVALUE PROBLEM OF NONSYMMETRIC REAL MATRICES

Quantum physicists are very familiar with the eigenvalue problem of symmetric real matrices and Hermitian complex matrices, but less familiar with the eigenproblem of real

nonsymmetric matrices. Therefore, here we summarize a few useful concepts and relations about the latter.

For concreteness, we consider a 3×3 real nonsymmetric matrix $\hat{\boldsymbol{M}}$, as in the main text. The complex number λ is an eigenvalue of $\hat{\boldsymbol{M}}$, if $\det(\hat{\boldsymbol{M}} - \lambda \mathbb{1}) = 0$. All eigenvalues of a real symmetric matrix are real, but this is not guaranteed if the matrix is nonsymmetric. The quantity $\det(\hat{\boldsymbol{M}} - \lambda \mathbb{1})$ is called the characteristic polynomial of $\hat{\boldsymbol{M}}$. According to the fundamental theorem of algebra, the characteristic polynomial can be factored into the product of three terms,

$$\det(\hat{\boldsymbol{M}} - \lambda \mathbb{1}) = (\lambda_1 - \lambda)(\lambda_2 - \lambda)(\lambda_3 - \lambda), \tag{A1}$$

where λ_i's are the eigenvalues of $\hat{\boldsymbol{M}}$.

The algebraic multiplicity $\mu(\lambda_i)$ of the eigenvalue λ_i is its multiplicity as a root of the characteristic polynomial. The geometric multiplicity $\gamma(\lambda_i)$ is the maximal number of linearly independent eigenvectors belonging to the eigenvalue λ_i, that is, the dimension of the eigensubspace corresponding to λ_i. For generic 3×3 matrices, it holds that $1 \leqslant \gamma(\lambda_i) \leqslant \mu(\lambda_i) \leqslant 3$, while for real symmetric and complex Hermitian matrices, it holds that $1 \leqslant \gamma(\lambda_i) = \mu(\lambda_i) \leqslant 3$.

A real symmetric (complex Hermitian) matrix can always be diagonalized with an orthogonal (unitary) transformation, whose matrix is constructed from the eigenvectors. This is not the case for a real nonsymmetric matrix. Nevertheless, there is still a canonical form $\hat{\boldsymbol{J}}$ of a real nonsymmetric matrix $\hat{\boldsymbol{M}}$, called the Jordan normal form (see the examples in Table I). The Jordan normal form is not diagonal, but it has a block-diagonal structure, and this structure is related to the algebraic and geometrical multiplicities of $\hat{\boldsymbol{M}}$. If the matrix has a size greater than 3, then the eigenvalues and their algebraic and geometric multiplicities are in general not sufficient to determine the Jordan normal form of the matrix. But in our case, when $\hat{\boldsymbol{M}}$ is a 3×3 matrix, the eigenvalues and the multiplicities do determine the Jordan normal form: each eigenvalue λ_i has a block in the Jordan normal form with the size of its algebraic multiplicity $\mu(\lambda_i)$, and within each block, there are as many 1 entries on the superdiagonal as the difference $\mu(\lambda_i) - \gamma(\lambda_i)$ between the algebraic and geometric multiplicities. In Table I, we list seven examples. The claim is that for any matrix $\hat{\boldsymbol{M}}$, there is a similarity transformation (invertible matrix) $\hat{\boldsymbol{P}}$, such that

$$\hat{\boldsymbol{J}} = \hat{\boldsymbol{P}}^{-1} \hat{\boldsymbol{M}} \hat{\boldsymbol{P}} \tag{A2}$$

is a Jordan normal form, and hence any matrix $\hat{\boldsymbol{M}}$ can be decomposed as in Eq. (8).

APPENDIX B: ROLE OF LOCAL SPIN BASIS TRANSFORMATIONS

Here, we collect a few facts and remarks about the role of local spin basis transformations in the spin-orbit-coupled two-spin problem studied in the main text. Some of these are used in our proofs.

Existence of a basis where the g tensors are symmetric. The Hamiltonian in Eq. (3) is built on a single-particle model [18] in which both sites support a single spinful orbital level, and the corresponding two states are Kramers degenerate at zero magnetic field. Because of this Kramers degeneracy, there is an ambiguity in choosing the basis states. The Hamiltonian in Eq. (3) is generic, i.e., this form is guaranteed no matter how we choose the basis. However, the actual secondary parameters (g-tensor matrix elements and the rotation matrix $\hat{\boldsymbol{R}}$) change if we change the basis.

First, we show that one can always choose a local spin basis in which the g tensors are symmetric. For this, we recall that any local spin basis transformation, apart from an arbitrary complex phase, can be written as a unitary operation [46]

$$U(\boldsymbol{\alpha}) = \exp(-i\alpha \boldsymbol{n} \cdot \boldsymbol{S}), \tag{B1}$$

where $\boldsymbol{\alpha}$ is a real three-component vector. Furthermore, this transformation corresponds to a rotation $\hat{\boldsymbol{O}}_{\boldsymbol{\alpha}}$ of the spin vector operator around the direction of $\boldsymbol{\alpha}$ with angle $\alpha = |\boldsymbol{\alpha}|$:

$$U(\boldsymbol{\alpha}) \boldsymbol{S} U(\boldsymbol{\alpha})^{\dagger} = \hat{\boldsymbol{O}}_{\boldsymbol{\alpha}}^{-1} \boldsymbol{S}. \tag{B2}$$

When we apply on our Hamiltonian H of Eq. (3) two different spin transformations on the two sites, U_{L} and U_{R}, which are represented by the rotations $\hat{\boldsymbol{O}}_{\mathrm{L}}$ and $\hat{\boldsymbol{O}}_{\mathrm{R}}$, respectively, then this combined transformation results in

$$\begin{aligned} H' &= (U_{\mathrm{L}} \otimes U_{\mathrm{R}}) H (U_{\mathrm{L}} \otimes U_{\mathrm{R}})^{\dagger} \\ &= \mu_{\mathrm{B}} \boldsymbol{B} \cdot \left(\hat{\boldsymbol{g}}_{\mathrm{L}} \hat{\boldsymbol{O}}_{\mathrm{L}}^{-1} \boldsymbol{S}_{\mathrm{L}} + \hat{\boldsymbol{g}}_{\mathrm{R}} \hat{\boldsymbol{O}}_{\mathrm{R}}^{-1} \boldsymbol{S}_{\mathrm{R}} \right) \\ &\quad + J \boldsymbol{S}_{\mathrm{L}} \cdot \hat{\boldsymbol{O}}_{\mathrm{L}} \hat{\boldsymbol{R}} \hat{\boldsymbol{O}}_{\mathrm{R}}^{-1} \boldsymbol{S}_{\mathrm{R}}. \end{aligned} \tag{B3}$$

Recall also that any real matrix has a polar decomposition to a symmetric real matrix and a rotation matrix, therefore, the g tensors can also be decomposed as $\hat{\boldsymbol{g}}_{\mathrm{L/R}} = \hat{\boldsymbol{G}}_{\mathrm{L/R}} \hat{\boldsymbol{Q}}_{\mathrm{L/R}}$, where $\hat{\boldsymbol{G}}_{\mathrm{L/R}}$ are real and symmetric and $\hat{\boldsymbol{Q}}_{\mathrm{L/R}}$ are rotations. For a g tensor with a positive (negative) determinant, we choose the polar decomposition whose real symmetric matrix $\hat{\boldsymbol{Q}}$ is positive (negative) definite. Then, by specifying the rotations in Eq. (B3) as $\hat{\boldsymbol{O}}_{\mathrm{L/R}} = \hat{\boldsymbol{Q}}_{\mathrm{L/R}}$, the transformed Hamiltonian reads as

$$\begin{aligned} H' &= \mu_{\mathrm{B}} \boldsymbol{B} \cdot (\hat{\boldsymbol{G}}_{\mathrm{L}} \boldsymbol{S}_{\mathrm{L}} + \hat{\boldsymbol{G}}_{\mathrm{R}} \boldsymbol{S}_{\mathrm{R}}) \\ &\quad + J \boldsymbol{S}_{\mathrm{L}} \cdot \hat{\boldsymbol{R}}' \boldsymbol{S}_{\mathrm{R}}, \end{aligned} \tag{B4}$$

where $\hat{\boldsymbol{R}}' = \hat{\boldsymbol{Q}}_{\mathrm{L}} \hat{\boldsymbol{R}} \hat{\boldsymbol{Q}}_{\mathrm{R}}^{-1}$.

An interesting feature of this particular basis choice is its strong relevance to spectroscopy experiments: if a spectroscopy experiment measures the Zeeman splitting as a function of the magnetic-field direction, then the principal axes and principal values of $\hat{\boldsymbol{G}}$ can be directly calculated from that data [50]. Another interesting feature of this basis is as follows. For concreteness, consider the case when $\det \hat{\boldsymbol{g}}_{\mathrm{L}}$ and $\det \hat{\boldsymbol{g}}_{\mathrm{R}}$ have positive determinants. Then, if the exchange rotation is sufficiently close to the identity, $\hat{\boldsymbol{R}}' \approx \mathbb{1}$, then the degeneracy points generically form the six-points pattern, due to the fact that the matrix $\hat{\boldsymbol{M}}$ converges to a real matrix that has only positive eigenvalues. This follows from the observation that in this particular case, the matrix $\hat{\boldsymbol{M}}$ is similar to $\hat{\boldsymbol{G}}_{\mathrm{R}}^{-1/2} \hat{\boldsymbol{M}} \hat{\boldsymbol{G}}_{\mathrm{R}}^{1/2} = \hat{\boldsymbol{G}}_{\mathrm{R}}^{-1/2} \hat{\boldsymbol{G}}_{\mathrm{L}} \hat{\boldsymbol{G}}_{\mathrm{R}}^{-1/2}$, the latter one is symmetric and positive definite, and hence its eigenvalues are positive. The same statement can be proven, with small modifications, for the case when both g tensors have negative determinants.

$\hat{\boldsymbol{M}}$ is invariant under any local spin transformation. In the main text, we have used the matrix $\hat{\boldsymbol{M}}$ to characterize the magnetic degeneracy points. It is a natural expectation that the locations of the degeneracy points do not depend on

the local spin basis choice. Can we prove this directly? Yes, and actually we can prove something stronger: the matrix $\hat{\boldsymbol{M}}$ itself is invariant under local spin basis transformations. This is a straightforward consequence of the transformation rules used above. A general basis transformation results in $\hat{\boldsymbol{g}}_{\mathrm{L/R}} \mapsto \hat{\boldsymbol{g}}_{\mathrm{L,R}}\hat{\boldsymbol{O}}_{\mathrm{L,R}}^{-1}$ and $\hat{\boldsymbol{R}} \mapsto \hat{\boldsymbol{O}}_{\mathrm{L}}\hat{\boldsymbol{R}}\hat{\boldsymbol{O}}_{\mathrm{R}}^{-1}$. Substituting these into the definition of $\hat{\boldsymbol{M}}$ we can get the transformed matrix as

$$\hat{\boldsymbol{M}} \mapsto \left(\hat{\boldsymbol{g}}_{\mathrm{L}}\hat{\boldsymbol{O}}_{\mathrm{L}}^{-1}\right)\left(\hat{\boldsymbol{O}}_{\mathrm{L}}\hat{\boldsymbol{R}}\hat{\boldsymbol{O}}_{\mathrm{R}}^{-1}\right)\left(\hat{\boldsymbol{O}}_{\mathrm{R}}\hat{\boldsymbol{g}}_{\mathrm{R}}^{-1}\right) = \hat{\boldsymbol{M}}, \tag{B5}$$

so $\hat{\boldsymbol{M}}$ is indeed invariant under local spin transformations as we expected.

APPENDIX C: LOCATIONS OF THE MAGNETIC DEGENERACY POINTS

Here, we outline how to determine the locations of the ground-state magnetic degeneracy points studied in the main text. First, we consider the case when the magnetic field vector $\boldsymbol{B} = B\boldsymbol{v}_a$ is a left eigenvector of $\hat{\boldsymbol{M}}$ with a positive eigenvalue a, and we assume that $\boldsymbol{v}_a$ is normalized. Then, the effective magnetic field vectors of Eq. (5) are parallel, $\boldsymbol{B}'_{\mathrm{L,eff}} \parallel \boldsymbol{B}'_{\mathrm{R,eff}}$, and point to the same direction

$$\tilde{\boldsymbol{v}}_a = \frac{\hat{\boldsymbol{g}}_{\mathrm{L}}^{\mathrm{T}}\boldsymbol{v}_a}{g_{\mathrm{L}}} = \frac{\hat{\boldsymbol{R}}\hat{\boldsymbol{g}}_{\mathrm{R}}^{\mathrm{T}}\boldsymbol{v}_a}{g_{\mathrm{R}}}, \tag{C1}$$

where $g_{\mathrm{L}} = |\hat{\boldsymbol{g}}_{\mathrm{L}}^{\mathrm{T}}\boldsymbol{v}_a|$ and $g_{\mathrm{R}} = |\hat{\boldsymbol{R}}\hat{\boldsymbol{g}}_{\mathrm{R}}^{\mathrm{T}}\boldsymbol{v}_a|$. Now, we do a second spin rotation $\mathcal{U}_2 = U_{\mathrm{L}}(\hat{\boldsymbol{O}}) \otimes U_{\mathrm{R}}(\hat{\boldsymbol{O}})$ on the Hamiltonian H' of Eq. (5), to make the direction of $\tilde{\boldsymbol{v}}_a$ the new spin quantization direction. That is,

$$\hat{\boldsymbol{O}}\tilde{\boldsymbol{v}}_a = \boldsymbol{e}_z, \tag{C2}$$

and $\hat{\boldsymbol{O}}$ can be chosen, e.g., as the π rotation around the bisector of $\tilde{\boldsymbol{v}}_a$ and the z axis. Here, the definition of U_{L} and U_{R} follows Eq. (4). Then, the spin quantization axis for both spin is redefined as the direction of the parallel effective magnetic fields. After this transformation, the Hamiltonian reads as

$$\begin{aligned} H'' &= \mathcal{U}_2 H' \mathcal{U}_2^{\dagger} \\ &= \mu_{\mathrm{B}}\boldsymbol{B}\cdot(\hat{\boldsymbol{g}}''_{\mathrm{L}}\boldsymbol{S}_{\mathrm{L}} + \hat{\boldsymbol{g}}''_{\mathrm{R}}\cdot\boldsymbol{S}_{\mathrm{R}}) + J\boldsymbol{S}_{\mathrm{L}}\cdot\boldsymbol{S}_{\mathrm{R}}, \end{aligned} \tag{C3}$$

where

$$\hat{\boldsymbol{g}}''_{\mathrm{L}} = \hat{\boldsymbol{g}}_{\mathrm{L}}\hat{\boldsymbol{O}}^{-1}, \tag{C4a}$$

$$\hat{\boldsymbol{g}}''_{\mathrm{R}} = \hat{\boldsymbol{g}}_{\mathrm{R}}\hat{\boldsymbol{R}}^{-1}\hat{\boldsymbol{O}}^{-1}. \tag{C4b}$$

The transformed Hamiltonian H'' with effective fields in the z direction reads as

$$H''_z = \mu_{\mathrm{B}}B(g_{\mathrm{L}}S_{\mathrm{L}z} + g_{\mathrm{R}}S_{\mathrm{R}z}) + J\boldsymbol{S}_{\mathrm{L}}\cdot\boldsymbol{S}_{\mathrm{R}}, \tag{C5}$$

where $g_{\mathrm{L,R}} = |\hat{\boldsymbol{g}}_{\mathrm{L,R}}^{\mathrm{T}}\boldsymbol{v}_a|$. Later we will use the fact that

$$g_{\mathrm{L}}/g_{\mathrm{R}} = a, \tag{C6}$$

which follows from $\boldsymbol{v}_a$ being a left eigenvector of $\hat{\boldsymbol{M}}$ with eigenvalue a:

$$\boldsymbol{v}_a^{\mathrm{T}}\hat{\boldsymbol{M}} = a\boldsymbol{v}_a^{\mathrm{T}}. \tag{C7}$$

This Hamiltonian H'' conserves the total spin projection $S_{\mathrm{tot},z} = S_{\mathrm{L}z} + S_{\mathrm{R}z}$, and thus has the following block-diagonal matrix form in the product basis $|\uparrow\uparrow\rangle, |\uparrow\downarrow\rangle, |\downarrow\uparrow\rangle, |\downarrow\downarrow\rangle$:

$$H''_z = \frac{1}{2}\begin{pmatrix} \mu_{\mathrm{B}}g_+B & 0 & 0 & 0 \\ 0 & \mu_{\mathrm{B}}g_-B - J & J & 0 \\ 0 & J & -\mu_{\mathrm{B}}g_-B - J & 0 \\ 0 & 0 & 0 & -\mu_{\mathrm{B}}g_+B \end{pmatrix}, \tag{C8}$$

where $g_{\pm} = g_{\mathrm{L}} \pm g_{\mathrm{R}}$. Energy eigenstates from different subspaces of $S_{\mathrm{tot},z}$ can be degenerate because there are no matrix elements mixing them.

At zero magnetic field, the ground state of H'' in Eq. (C8) is the singlet state $(|\uparrow\downarrow\rangle - |\downarrow\uparrow\rangle)/\sqrt{2}$ from the $S_{\mathrm{tot},z} = 0$ subspace, with energy $-J$, and the remaining three states are triplets with zero energy. If the magnetic field is much greater than the interaction strength J, then the energy eigenstates are the product states. The ground state is the state $|\downarrow\downarrow\rangle$ from the $S_{\mathrm{tot},z} = -1$ subspace with energy $-\frac{1}{2}\mu_{\mathrm{B}}g_+B$: this follows from that fact that $|g_+| > |g_-|$, which is implied by $g_{\mathrm{L}}, g_{\mathrm{R}} > 0$. Therefore, at a certain magnetic-field strength between zero and infinity, the $S_{\mathrm{tot},z} = 0$ ground state must be degenerate with the $S_{\mathrm{tot},z} = -1$ ground state. In fact, straightforward calculation shows that this level crossing degeneracy happens at the critical magnetic-field strength

$$B_a = \frac{J}{2\mu_B}\left(\frac{1}{g_{\mathrm{L}}} + \frac{1}{g_{\mathrm{R}}}\right), \tag{C9}$$

and the degenerate ground states are

$$|0\rangle = \frac{1}{\sqrt{g_{\mathrm{L}}^2 + g_{\mathrm{R}}^2}}(g_{\mathrm{R}}|\uparrow\downarrow\rangle - g_{\mathrm{L}}|\downarrow\uparrow\rangle), \tag{C10a}$$

$$|-1\rangle = |\downarrow\downarrow\rangle, \tag{C10b}$$

labeled with their $S_{\mathrm{tot},z}$ quantum number.

If, on the other hand, $\boldsymbol{B}$ is a left eigenvector of $\hat{\boldsymbol{M}}$ with a negative eigenvalue, then the effective magnetic fields $\boldsymbol{B}'_{\mathrm{L,eff}}$ and $\boldsymbol{B}'_{\mathrm{R,eff}}$ are antialigned. Then, the Hamiltonian can be brought to the same form as in Eq. (C8), with the change that now $|g_+| < |g_-|$. Therefore, the ground states in the limits of zero and large magnetic fields are both in the $S_{\mathrm{tot},z} = 0$ subspace, and there is no ground-state level crossing.

APPENDIX D: CLOSED DEGENERACY LINES ARE ELLIPSES, CLOSED DEGENERACY SURFACES ARE ELLIPSOIDS

In Table I, the eigenpattern (IV) implies that the degeneracy points form a closed surface. Here, we show that this surface is an ellipsoid. A similar proof shows that the loops formed by the degeneracy points in cases (II), (V), and (X) are ellipses.

In case (IV), the matrix $\hat{\boldsymbol{M}}$ has a single eigenvalue a and the normalized eigenvectors form the three-dimensional unit sphere. So, any $\boldsymbol{v}$ unit vector is an eigenvector, and we can apply the results (C6) and (C9) to obtain the locations of the degeneracy points

$$\boldsymbol{B}_a(\boldsymbol{v}) = \frac{J(1+a)}{2\mu_{\mathrm{B}}}\frac{\boldsymbol{v}}{|\hat{\boldsymbol{g}}_{\mathrm{L}}^{\mathrm{T}}\boldsymbol{v}|} = \frac{J(1+a)}{2\mu_{\mathrm{B}}}\frac{\boldsymbol{v}}{|\hat{\boldsymbol{G}}_{\mathrm{L}}\boldsymbol{v}|}. \tag{D1}$$

In the second step, we have made use of the polar decomposition of $\hat{\boldsymbol{g}}_{\mathrm{L}}$, introduced in Appendix B, where $\hat{\boldsymbol{G}}_{\mathrm{L}}$ denotes the

real symmetric component. In the principal reference frame of $\hat{\boldsymbol{G}}_{\mathrm{L}}$, the location of the degeneracy point associated to $\boldsymbol{v}$ reads as

$$\begin{pmatrix} B_{ax} \\ B_{ay} \\ B_{az} \end{pmatrix} = \frac{J(1+a)}{2\mu_{\mathrm{B}}} \frac{1}{\sqrt{G_x^2 v_x^2 + G_y^2 v_y^2 + G_z^2 v_z^2}} \begin{pmatrix} v_x \\ v_y \\ v_z \end{pmatrix}, \quad \text{(D2)}$$

where (G_x, G_y, G_z) are the principal values of $\hat{\boldsymbol{G}}_{\mathrm{L}}$. Acting with $\hat{\boldsymbol{G}}_{\mathrm{L}}$ on both sides of the equation, and taking the length squared of the resulting vectors, we obtain the equation

$$G_x^2 B_{ax}^2 + G_y^2 B_{ay}^2 + G_z^2 B_{az}^2 = \left[\frac{J(1+a)}{2\mu_{\mathrm{B}}}\right]^2, \quad \text{(D3)}$$

which implies that the degeneracy points form an ellipsoid.

For cases (II), (V), and (X), we have an additional constraint: $\boldsymbol{v}$ has to be in the degenerate subspace of $\hat{\boldsymbol{M}}$. This intersects the ellipsoid with a plane passing through the origin. Since the intersection of a plane and an ellipsoid is always an ellipse, we conclude that the degeneracy points in these cases are ellipses.

APPENDIX E: TOPOLOGICAL CHARGE DISTRIBUTIONS

Here, we provide the derivation of the topological charges associated to the ground-state magnetic degeneracy points. The results were summarized in Tables I and II in the main text. The first, simple step of the derivation is to approximate the Hamiltonian in the vicinity of the degeneracy point and truncate it to the two-dimensional degenerate subspace of interest. A second, nontrivial step is to connect this two-dimensional Hamiltonian to the eigenvalue problem of the matrix $\hat{\boldsymbol{M}}$. In the third step, this allows us to express the topological charges of the degeneracy points via the eigenvalues of $\hat{\boldsymbol{M}}$, using the matrix determinant lemma.

To exemplify the derivation, consider the case when the total topological charge is $\mathcal{Q} = +2$, and the eigenpattern of $\hat{\boldsymbol{M}}$ is (I) (see Table I). Then, $\hat{\boldsymbol{M}}$ has three eigenvalues a, b, c, three eigenvectors $\boldsymbol{v}_a$, $\boldsymbol{v}_b$, $\boldsymbol{v}_c$, and the set of the ground-state magnetic degeneracy points is formed by six Weyl points. For this case, we will not only show that the distribution of topological charge among the six degeneracy points is $4 \times (+1)$, $2 \times (-1)$, but also that the negatively charged point pair belongs to the eigenvalue that is between the other two eigenvalues.

To calculate the topological charge of a Weyl point, say, $\boldsymbol{B}_{a+}$, we focus on the two degenerate ground states $|0\rangle$ and $|-1\rangle$ in the degeneracy point [see Eqs. (C10)], make a linear expansion of the Hamiltonian for small deviations $\delta\boldsymbol{B} = \boldsymbol{B} - \boldsymbol{B}_{a+}$ of the magnetic field from the degeneracy point, and truncate the Hamiltonian for the two-dimensional subspace spanned by $|0\rangle$ and $|-1\rangle$. This reduced Hamiltonian can be written in terms of Pauli matrices

$$H_{\mathrm{red}}(\delta\boldsymbol{B}) = \mu_{\mathrm{B}}\, \delta\boldsymbol{B} \cdot \hat{\boldsymbol{g}}_{a+}\boldsymbol{\tau}, \quad \text{(E1)}$$

where $\boldsymbol{\tau} = (\tau_1, \tau_2, \tau_3)$ is half times the vector of Pauli matrices, e.g., $\tau_3 = \frac{1}{2}(|0\rangle\langle 0| - |-1\rangle\langle -1|)$. Because of the similarity of H_{red} and the Hamiltonian of a spin in a magnetic field with an anisotropic g tensor, we call $\hat{\boldsymbol{g}}_{a+}$ the *effective g tensor* of the degeneracy point $\boldsymbol{B}_{a+}$. The determinant of the effective g tensor of a Weyl point is nonzero, and its sign provides the topological charge of the Weyl point:

$$\mathcal{Q}_{a+} = \mathrm{sgn}\det(\hat{\boldsymbol{g}}_{a+}). \quad \text{(E2)}$$

To obtain an analytical result for the elements of the effective g tensor, we evaluate H_{red} in Eq. (E1) with $\delta\boldsymbol{B} = \delta B \boldsymbol{e}_\alpha$ ($\alpha = x, y, z$) pointing along the unit vector $\boldsymbol{e}_\alpha$ of direction α, multiply both sides with τ_β ($\beta = x, y, z$), and take the trace of both sides. This procedure yields the matrix elements

$$(\hat{\boldsymbol{g}}_{a+})_{\alpha\beta} = \frac{2}{\mu_{\mathrm{B}}\, \delta B}\mathrm{Tr}[H_{\mathrm{red}}(\delta B\, \boldsymbol{e}_\alpha)\tau_\beta]. \quad \text{(E3)}$$

The matrix obtained from this relation can be identified with this expression:

$$\hat{\boldsymbol{g}}_{a+} = \frac{g_{\mathrm{R}}^2 \hat{\boldsymbol{g}}_{\mathrm{L}}'' + g_{\mathrm{L}}^2 \hat{\boldsymbol{g}}_{\mathrm{R}}''}{g_{\mathrm{L}}^2 + g_{\mathrm{R}}^2} \boldsymbol{e}_z \otimes \boldsymbol{e}_z + \frac{g_{\mathrm{R}} \hat{\boldsymbol{g}}_{\mathrm{L}}'' - g_{\mathrm{L}} \hat{\boldsymbol{g}}_{\mathrm{R}}''}{\sqrt{g_{\mathrm{L}}^2 + g_{\mathrm{R}}^2}} (\mathbb{1} - \boldsymbol{e}_z \otimes \boldsymbol{e}_z). \quad \text{(E4)}$$

Note that from now on, $\otimes$ denotes the dyadic product of two three-dimensional real vectors.

To calculate the topological charge $\mathcal{Q}_{a+}$ of Eq. (E2), we calculate here $\det(\hat{\boldsymbol{g}}_{a+}\hat{\boldsymbol{O}})$, whose sign provides $\mathcal{Q}_{a+}$ as $\hat{\boldsymbol{O}}$ is a rotation. Recall that $\hat{\boldsymbol{O}}$ is the rotation setting the z axis along the direction of $\hat{\boldsymbol{R}}\hat{\boldsymbol{g}}_{\mathrm{R}}^{\mathrm{T}}\boldsymbol{v}_a$ (which is the same as the direction of $\hat{\boldsymbol{g}}_{\mathrm{L}}^{\mathrm{T}}\boldsymbol{v}_a$). We calculate $\det(\hat{\boldsymbol{g}}_{a+}\hat{\boldsymbol{O}})$ via a lengthy but straightforward application of the definitions, and the only nontrivial step will be the usage of a special version of the matrix determinant lemma.

Inserting the relations in Eq. (C4) into Eq. (E4), we obtain

$$\hat{\boldsymbol{g}}_{a+} = \frac{g_{\mathrm{R}}^2 \hat{\boldsymbol{g}}_{\mathrm{L}} \hat{\boldsymbol{O}}^{-1} + g_{\mathrm{L}}^2 \hat{\boldsymbol{g}}_{\mathrm{R}} \hat{\boldsymbol{R}}^{-1} \hat{\boldsymbol{O}}^{-1}}{g_{\mathrm{L}}^2 + g_{\mathrm{R}}^2} \boldsymbol{e}_z \otimes \boldsymbol{e}_z + \frac{g_{\mathrm{R}} \hat{\boldsymbol{g}}_{\mathrm{L}} \hat{\boldsymbol{O}}^{-1} - g_{\mathrm{L}} \hat{\boldsymbol{g}}_{\mathrm{R}} \hat{\boldsymbol{R}}^{-1} \hat{\boldsymbol{O}}^{-1}}{\sqrt{g_{\mathrm{L}}^2 + g_{\mathrm{R}}^2}} (\mathbb{1} - \boldsymbol{e}_z \otimes \boldsymbol{e}_z). \quad \text{(E5)}$$

Multiplying both sides of Eq. (E5) with $\hat{\boldsymbol{O}}$ from the right results in

$$\hat{\boldsymbol{g}}_{a+}\hat{\boldsymbol{O}} = \frac{g_{\mathrm{R}}^2 \hat{\boldsymbol{g}}_{\mathrm{L}} + g_{\mathrm{L}}^2 \hat{\boldsymbol{g}}_{\mathrm{R}} \hat{\boldsymbol{R}}^{-1}}{g_{\mathrm{L}}^2 + g_{\mathrm{R}}^2} \hat{\boldsymbol{O}}^{-1} \boldsymbol{e}_z \otimes \boldsymbol{e}_z \hat{\boldsymbol{O}} + \frac{g_{\mathrm{R}} \hat{\boldsymbol{g}}_{\mathrm{L}} - g_{\mathrm{L}} \hat{\boldsymbol{g}}_{\mathrm{R}} \hat{\boldsymbol{R}}^{-1}}{\sqrt{g_{\mathrm{L}}^2 + g_{\mathrm{R}}^2}} \hat{\boldsymbol{O}}^{-1} (\mathbb{1} - \boldsymbol{e}_z \otimes \boldsymbol{e}_z) \hat{\boldsymbol{O}}. \quad \text{(E6)}$$

From Eq. (C2), we see that $\tilde{\boldsymbol{v}}_a = \hat{\boldsymbol{O}}^{-1}\boldsymbol{e}_z$, and hence we have

$$\hat{\boldsymbol{g}}_{a+}\hat{\boldsymbol{O}} = \frac{g_{\mathrm{R}}^2 \hat{\boldsymbol{g}}_{\mathrm{L}} + g_{\mathrm{L}}^2 \hat{\boldsymbol{g}}_{\mathrm{R}} \hat{\boldsymbol{R}}^{-1}}{g_{\mathrm{L}}^2 + g_{\mathrm{R}}^2} \tilde{\boldsymbol{v}}_a \otimes \tilde{\boldsymbol{v}}_a + \frac{g_{\mathrm{R}} \hat{\boldsymbol{g}}_{\mathrm{L}} - g_{\mathrm{L}} \hat{\boldsymbol{g}}_{\mathrm{R}} \hat{\boldsymbol{R}}^{-1}}{\sqrt{g_{\mathrm{L}}^2 + g_{\mathrm{R}}^2}} (\mathbb{1} - \tilde{\boldsymbol{v}}_a \otimes \tilde{\boldsymbol{v}}_a). \quad \text{(E7)}$$

Dividing both the numerators and the denominators by g_{R}^2, we have

$$\hat{\boldsymbol{g}}_{a+}\hat{\boldsymbol{O}} = \frac{\hat{\boldsymbol{g}}_{\mathrm{L}} + \frac{g_{\mathrm{L}}^2}{g_{\mathrm{R}}^2}\hat{\boldsymbol{g}}_{\mathrm{R}}\hat{\boldsymbol{R}}^{-1}}{1+\frac{g_{\mathrm{L}}^2}{g_{\mathrm{R}}^2}}\tilde{\boldsymbol{v}}_a \otimes \tilde{\boldsymbol{v}}_a + \frac{\hat{\boldsymbol{g}}_{\mathrm{L}} - \frac{g_{\mathrm{L}}}{g_{\mathrm{R}}}\hat{\boldsymbol{g}}_{\mathrm{R}}\hat{\boldsymbol{R}}^{-1}}{\sqrt{1+\frac{g_{\mathrm{L}}^2}{g_{\mathrm{R}}^2}}}(\mathbb{1} - \tilde{\boldsymbol{v}}_a \otimes \tilde{\boldsymbol{v}}_a). \tag{E8}$$

Using the relation Eq. (C6), this simplifies to

$$\hat{\boldsymbol{g}}_{a+}\hat{\boldsymbol{O}} = \frac{\hat{\boldsymbol{g}}_{\mathrm{L}} + a^2\hat{\boldsymbol{g}}_{\mathrm{R}}\hat{\boldsymbol{R}}^{-1}}{1+a^2}\tilde{\boldsymbol{v}}_a \otimes \tilde{\boldsymbol{v}}_a + \frac{\hat{\boldsymbol{g}}_{\mathrm{L}} - a\hat{\boldsymbol{g}}_{\mathrm{R}}\hat{\boldsymbol{R}}^{-1}}{\sqrt{1+a^2}}(\mathbb{1} - \tilde{\boldsymbol{v}}_a \otimes \tilde{\boldsymbol{v}}_a). \tag{E9}$$

Inserting the unit matrix as $\mathbb{1}_{3\times3} = \hat{\boldsymbol{R}}\hat{\boldsymbol{g}}_{\mathrm{R}}^{-1}\hat{\boldsymbol{g}}_{\mathrm{R}}\hat{\boldsymbol{R}}^{-1}$ on the right of $\hat{\boldsymbol{g}}_{\mathrm{L}}$, we obtain

$$\hat{\boldsymbol{g}}_{a+}\hat{\boldsymbol{O}} = \frac{\hat{\boldsymbol{g}}_{\mathrm{L}}\hat{\boldsymbol{R}}\hat{\boldsymbol{g}}_{\mathrm{R}}^{-1}\hat{\boldsymbol{g}}_{\mathrm{R}}\hat{\boldsymbol{R}}^{-1} + a^2\hat{\boldsymbol{g}}_{\mathrm{R}}\hat{\boldsymbol{R}}^{-1}}{1+a^2}\tilde{\boldsymbol{v}}_a \otimes \tilde{\boldsymbol{v}}_a + \frac{\hat{\boldsymbol{g}}_{\mathrm{L}}\hat{\boldsymbol{R}}\hat{\boldsymbol{g}}_{\mathrm{R}}^{-1}\hat{\boldsymbol{g}}_{\mathrm{R}}\hat{\boldsymbol{R}}^{-1} - a\hat{\boldsymbol{g}}_{\mathrm{R}}\hat{\boldsymbol{R}}^{-1}}{\sqrt{1+a^2}}(\mathbb{1} - \tilde{\boldsymbol{v}}_a \otimes \tilde{\boldsymbol{v}}_a). \tag{E10}$$

Using the earlier definition $\hat{\boldsymbol{M}} = \hat{\boldsymbol{g}}_{\mathrm{L}}\hat{\boldsymbol{R}}\hat{\boldsymbol{g}}_{\mathrm{R}}^{-1}$ from Eq. (6), we find

$$\hat{\boldsymbol{g}}_{a+}\hat{\boldsymbol{O}} = \frac{\hat{\boldsymbol{M}} + a^2}{1+a^2}\hat{\boldsymbol{g}}_{\mathrm{R}}\hat{\boldsymbol{R}}^{-1}\tilde{\boldsymbol{v}}_a \otimes \tilde{\boldsymbol{v}}_a + \frac{\hat{\boldsymbol{M}} - a}{\sqrt{1+a^2}}\hat{\boldsymbol{g}}_{\mathrm{R}}\hat{\boldsymbol{R}}^{-1}(\mathbb{1} - \tilde{\boldsymbol{v}}_a \otimes \tilde{\boldsymbol{v}}_a).$$

Now, we rearrange the terms to express $\hat{\boldsymbol{g}}_{a+}\hat{\boldsymbol{O}}$ as the sum of a matrix and a dyadic product, a form revealing the applicability of the matrix determinant lemma:

$$\hat{\boldsymbol{g}}_{a+}\hat{\boldsymbol{O}} = \frac{\hat{\boldsymbol{M}} - a}{\sqrt{1+a^2}}\hat{\boldsymbol{g}}_{\mathrm{R}}\hat{\boldsymbol{R}}^{-1} + \left[\left(\frac{\hat{\boldsymbol{M}} + a^2}{1+a^2} - \frac{\hat{\boldsymbol{M}} - a}{\sqrt{1+a^2}}\right)\hat{\boldsymbol{g}}_{\mathrm{R}}\hat{\boldsymbol{R}}^{-1}\tilde{\boldsymbol{v}}_a\right] \otimes \tilde{\boldsymbol{v}}_a. \tag{E11}$$

The matrix determinant lemma states that for an invertible matrix $\hat{\boldsymbol{A}}$ and two vectors $\boldsymbol{u}$ and $\boldsymbol{v}$, it holds that

$$\det(\hat{\boldsymbol{A}} + \boldsymbol{u} \otimes \boldsymbol{v}) = (1 + \boldsymbol{v} \cdot \hat{\boldsymbol{A}}^{-1}\boldsymbol{u}) \det \hat{\boldsymbol{A}}. \tag{E12}$$

It is tempting to identify the quantities of Eq. (E11) with those appearing in the matrix determinant lemma (E12) as follows:

$$\hat{\boldsymbol{A}} = \frac{\hat{\boldsymbol{M}} - a}{\sqrt{1+a^2}}\hat{\boldsymbol{g}}_{\mathrm{R}}\hat{\boldsymbol{R}}^{-1}, \tag{E13a}$$

$$\hat{\boldsymbol{B}} = \frac{\hat{\boldsymbol{M}} + a^2}{1+a^2}\hat{\boldsymbol{g}}_{\mathrm{R}}\hat{\boldsymbol{R}}^{-1}, \tag{E13b}$$

$$\boldsymbol{u} = \left(\frac{\hat{\boldsymbol{M}} + a^2}{1+a^2} - \frac{\hat{\boldsymbol{M}} - a}{\sqrt{1+a^2}}\right)\hat{\boldsymbol{g}}_{\mathrm{R}}\hat{\boldsymbol{R}}^{-1}\tilde{\boldsymbol{v}}_a = (\hat{\boldsymbol{B}} - \hat{\boldsymbol{A}})\tilde{\boldsymbol{v}}_a, \tag{E13c}$$

$$\boldsymbol{v} = \tilde{\boldsymbol{v}}_a. \tag{E13d}$$

An important caveat is that our matrix $\hat{\boldsymbol{A}}$ is not invertible since a is one of the eigenvalues of $\hat{\boldsymbol{M}}$. Therefore, we can not use the matrix determinant lemma directly. Therefore, we will use the matrix determinant lemma for auxiliary quantities $\hat{\boldsymbol{A}}'$ and $\boldsymbol{u}'$ that are infinitesimally close to $\hat{\boldsymbol{A}}'$ and $\boldsymbol{u}'$, respectively, defining $\hat{\boldsymbol{A}}'$ as an invertible matrix, and take the limit $\hat{\boldsymbol{A}}' \to \hat{\boldsymbol{A}}$ and $\boldsymbol{u}' \to \boldsymbol{u}$ as the last step of the calculation. We define the auxiliary quantities as follows:

$$\hat{\boldsymbol{A}}' = \frac{\hat{\boldsymbol{M}} - a'}{\sqrt{1+a^2}}\hat{\boldsymbol{g}}_{\mathrm{R}}\hat{\boldsymbol{R}}^{-1}, \tag{E14}$$

$$\boldsymbol{u}' = (\hat{\boldsymbol{B}} - \hat{\boldsymbol{A}}')\tilde{\boldsymbol{v}}_a, \tag{E15}$$

and we will take the limit $a' \to a$ as the last step of the calculation.

Now, we use the matrix determinant lemma for $\hat{\boldsymbol{A}}'$, $\boldsymbol{u}'$, and $\boldsymbol{v}$ to evaluate the determinant of Eq. (E11), and express $\boldsymbol{u}'$ and $\boldsymbol{v}$ via Eqs. (E15) and (E13d), respectively:

$$\det \hat{\boldsymbol{g}}_{a+}\hat{\boldsymbol{O}} = [1 + \tilde{\boldsymbol{v}}_a \cdot \hat{\boldsymbol{A}}'^{-1}(\hat{\boldsymbol{B}} - \hat{\boldsymbol{A}}')\tilde{\boldsymbol{v}}_a] \det \hat{\boldsymbol{A}}'. \tag{E16}$$

We use in Eq. (E16) the fact that $\hat{\boldsymbol{O}}$ is a rotation, which implies $\det \hat{\boldsymbol{O}} = 1$, and furthermore we use the relations $\hat{\boldsymbol{A}}'^{-1}\hat{\boldsymbol{A}}' = \mathbb{1}_{3\times3}$ and $\tilde{\boldsymbol{v}}_a \cdot \tilde{\boldsymbol{v}}_a = 1$ to obtain

$$\det \hat{\boldsymbol{g}}_{a+} = \tilde{\boldsymbol{v}}_a \cdot \hat{\boldsymbol{A}}'^{-1}\hat{\boldsymbol{B}}\tilde{\boldsymbol{v}}_a \det \hat{\boldsymbol{A}}'. \tag{E17}$$

Then, $\hat{\boldsymbol{A}}'$ is expressed using Eq. (E14):

$$\det \hat{\boldsymbol{g}}_{a+} = \tilde{\boldsymbol{v}}_a \cdot \left(\frac{\hat{\boldsymbol{M}} - a'}{\sqrt{1+a^2}}\hat{\boldsymbol{g}}_{\mathrm{R}}\hat{\boldsymbol{R}}^{-1}\right)^{-1}\frac{\hat{\boldsymbol{M}} + a^2}{1+a^2}\hat{\boldsymbol{g}}_{\mathrm{R}}\hat{\boldsymbol{R}}^{-1}\tilde{\boldsymbol{v}}_a \times \det\left(\frac{\hat{\boldsymbol{M}} - a'}{\sqrt{1+a^2}}\hat{\boldsymbol{g}}_{\mathrm{R}}\hat{\boldsymbol{R}}^{-1}\right). \tag{E18}$$

Using the relation for the inverse of a matrix product, we rearrange the first matrix inverse to obtain

$$\det \hat{\boldsymbol{g}}_{a+} = \tilde{\boldsymbol{v}}_a \cdot \hat{\boldsymbol{R}}\hat{\boldsymbol{g}}_{\mathrm{R}}^{-1}\left(\frac{\hat{\boldsymbol{M}} - a'}{\sqrt{1+a^2}}\right)^{-1}\frac{\hat{\boldsymbol{M}} + a^2}{1+a^2}\hat{\boldsymbol{g}}_{\mathrm{R}}\hat{\boldsymbol{R}}^{-1}\tilde{\boldsymbol{v}}_a \times \det\left(\frac{\hat{\boldsymbol{M}} - a'}{\sqrt{1+a^2}}\hat{\boldsymbol{g}}_{\mathrm{R}}\hat{\boldsymbol{R}}^{-1}\right). \tag{E19}$$

Now, we use Eq. (C1), yielding

$$\det \hat{\boldsymbol{g}}_{a+} = \frac{\boldsymbol{v}_a}{g_{\mathrm{R}}} \cdot \left[\left(\frac{\hat{\boldsymbol{M}} - a'}{\sqrt{1+a^2}}\right)^{-1}\frac{\hat{\boldsymbol{M}} + a^2}{1+a^2}\right]\hat{\boldsymbol{g}}_{\mathrm{R}}\hat{\boldsymbol{R}}^{-1}\tilde{\boldsymbol{v}}_a \times \det\left(\frac{\hat{\boldsymbol{M}} - a'}{\sqrt{1+a^2}}\hat{\boldsymbol{g}}_{\mathrm{R}}\hat{\boldsymbol{R}}^{-1}\right). \tag{E20}$$

The next step is to make use of the fact that $\boldsymbol{v}_a$ is a left eigenvector of $\hat{\boldsymbol{M}}$ with eigenvalue a from Eq. (C7), that is, $\boldsymbol{v}_a^{\mathrm{T}}\hat{\boldsymbol{M}} = a\boldsymbol{v}_a^{\mathrm{T}}$:

$$\det \hat{\boldsymbol{g}}_{a+} = \left[\left(\frac{a - a'}{\sqrt{1+a^2}}\right)^{-1}\frac{a + a^2}{1+a^2}\right]\frac{1}{g_{\mathrm{R}}}\boldsymbol{v}_a \cdot \hat{\boldsymbol{g}}_{\mathrm{R}}\hat{\boldsymbol{R}}^{-1}\tilde{\boldsymbol{v}}_a \times \det\left(\frac{\hat{\boldsymbol{M}} - a'}{\sqrt{1+a^2}}\hat{\boldsymbol{g}}_{\mathrm{R}}\hat{\boldsymbol{R}}^{-1}\right). \tag{E21}$$

Expressing $\boldsymbol{v}_a$ from Eq. (C1), inserting that into Eq. (E21), and using $\tilde{\boldsymbol{v}}_a \cdot \tilde{\boldsymbol{v}}_a = 1$, we find

$$\det \hat{\boldsymbol{g}}_{a+} = \frac{\sqrt{1+a^2}}{a-a'}\frac{a+a^2}{1+a^2} \times \det\left(\frac{\hat{\boldsymbol{M}}-a'}{\sqrt{1+a^2}}\right)\det \hat{\boldsymbol{g}}_{\mathrm{R}} \det \hat{\boldsymbol{R}}^{-1}. \quad \text{(E22)}$$

Finally, expressing the first determinant via the eigenvalues, and invoking $\det \boldsymbol{R}^{-1} = 1$, we obtain

$$\det \hat{\boldsymbol{g}}_{a+} = \frac{\sqrt{1+a^2}}{a-a'}\frac{a+a^2}{1+a^2}\frac{(a-a')(b-a')(c-a')}{(\sqrt{1+a^2})^3}\det \hat{\boldsymbol{g}}_{\mathrm{R}} = \frac{a(1+a)}{(1+a^2)^2}(a-b)(a-c)\det \hat{\boldsymbol{g}}_{\mathrm{R}}, \quad \text{(E23)}$$

where the $a' \to a$ limit was taken in the last step.

Inserting this determinant into Eq. (E2) and using $a > 0$ and $\det \hat{\boldsymbol{g}}_{\mathrm{R}} > 0$, we obtain

$$\mathcal{Q}_{a+} = \mathrm{sgn}[(a-b)(a-c)]. \quad \text{(E24)}$$

The same result is obtained for $\mathcal{Q}_{a-}$, and analogous results are obtained for the remaining four degeneracy points:

$$\mathcal{Q}_{b\pm} = \mathrm{sgn}[(b-a)(b-c)], \quad \text{(E25)}$$

$$\mathcal{Q}_{c\pm} = \mathrm{sgn}[(c-a)(c-b)]. \quad \text{(E26)}$$

The results (E24), (E25), and (E26) imply that for the eigenpattern (I), the distribution of topological charge among the six degeneracy points is $4 \times (+1)$, $2 \times (-1)$, and that the negatively charged point pair belongs to the eigenvalue that is between the other two eigenvalues.

For the eigenpatterns (II) and (III), the two Weyl points belonging to the nondegenerate eigenvalue b can be analyzed in an analogous fashion, with the result that their topological charge is $+1$. As a natural consequence of this and the sum rule that the total topological charge is $+2$, the remaining degeneracy points, that is, the ellipse in case (II) and the two remaining points in case (III), must have zero topological charge. For the remaining eigenpatterns from (III) to (VII), the distribution of the total topological charge $+2$ is obvious.

We note that the result (E23) is valid not only for Weyl points, but for any ground-state magnetic degeneracy point. This has interesting implications regarding the energy dispersion in the vicinity of a degeneracy point $\boldsymbol{B}_{a+}$ whenever that point is in an eigenspace of $\hat{\boldsymbol{M}}$ that belongs to a degenerate eigenvalue a. In that case, the degeneracy of a implies that the right-hand side of (E23) yields zero, i.e., there is at least one direction for $\delta\boldsymbol{B}$ along which the dispersion is nonlinear. In cases (II), (IV), (V), and (IX), naturally, the special nondispersive directions are the tangents of the ellipse and the ellipsoid. However, it is remarkable that discrete degeneracy points can also have nonlinear dispersion. Examples are the two points in case (VI) with nonzero charge and the neutral points in cases (III) and (X). Degeneracy points showing similar nonlinear dispersion are sometimes called multi-Weyl points [32,42–44] in the literature. In general, their topological charges cannot be determined by their effective g tensor: for example, in case (VI), the determinants of the effective g tensors of the two degeneracy points are zero, nevertheless, each point has a topological charge $+1$.

[1] W. Wernsdorfer and R. Sessoli, Quantum phase interference and parity effects in magnetic molecular clusters, Science **284**, 133 (1999).

[2] A. Garg, Berry phases near degeneracies: Beyond the simplest case, Am. J. Phys. **78**, 661 (2010).

[3] P. Bruno, Berry Phase, Topology, and Degeneracies in Quantum Nanomagnets, Phys. Rev. Lett. **96**, 117208 (2006).

[4] R. Wiesendanger, Spin mapping at the nanoscale and atomic scale, Rev. Mod. Phys. **81**, 1495 (2009).

[5] A. Spinelli, M. Gerrits, R. Toskovic, B. Bryant, M. Ternes, and A. F. Otte, Exploring the phase diagram of the two-impurity Kondo problem, Nat. Commun. **6**, 10046 (2015).

[6] R. Hanson, L. P. Kouwenhoven, J. R. Petta, S. Tarucha, and L. M. K. Vandersypen, Spins in few-electron quantum dots, Rev. Mod. Phys. **79**, 1217 (2007).

[7] F. A. Zwanenburg, A. S. Dzurak, A. Morello, M. Y. Simmons, L. C. L. Hollenberg, G. Klimeck, S. Rogge, S. N. Coppersmith, and M. A. Eriksson, Silicon quantum electronics, Rev. Mod. Phys. **85**, 961 (2013).

[8] M. V. Berry, Quantal phase factors accompanying adiabatic changes, Proc. R. Soc. Lond. A **392**, 45 (1984).

[9] F. Wilczek and A. Shapere, *Geometric Phases in Physics*, Vol. 5 (World Scientific, Singapore, 1989).

[10] P. San-Jose, B. Scharfenberger, G. Schön, A. Shnirman, and G. Zarand, Geometric phases in semiconductor spin qubits: Manipulations and decoherence, Phys. Rev. B **77**, 045305 (2008).

[11] P. San-Jose, G. Zarand, A. Shnirman, and G. Schön, Geometrical Spin Dephasing in Quantum Dots, Phys. Rev. Lett. **97**, 076803 (2006).

[12] K. v. Klitzing, G. Dorda, and M. Pepper, New Method for High-Accuracy Determination of the Fine-Structure Constant Based on Quantized Hall Resistance, Phys. Rev. Lett. **45**, 494 (1980).

[13] D. J. Thouless, M. Kohmoto, M. P. Nightingale, and M. den Nijs, Quantized Hall Conductance in a Two-Dimensional Periodic Potential, Phys. Rev. Lett. **49**, 405 (1982).

[14] J. von Neumann and E. P. Wigner, Über das Verhalten von Eigenwerten bei adiabatischen Prozessen, Phys. Z. **30**, 467 (1929).

[15] C. Herring, Accidental degeneracy in the energy bands of crystals, Phys. Rev. **52**, 365 (1937).

[16] V. Gritsev and A. Polkovnikov, Dynamical quantum Hall effect in the parameter space, Proc. Natl. Acad. Sci. U. S. A. **109**, 6457 (2012).

[17] P. Roushan, C. Neill, Yu Chen, M. Kolodrubetz, C. Quintana, N. Leung, M. Fang, R. Barends, B. Campbell, Z. Chen, B. Chiaro,

A. Dunsworth, E. Jeffrey, J. Kelly, A. Megrant, J. Mutus, P. J. J. O'Malley, D. Sank, A. Vainsencher, J. Wenner *et al.*, Observation of topological transitions in interacting quantum circuits, Nature (London) **515**, 241 (2014).

[18] Z. Scherübl, A. Pályi, G. Frank, I. E. Lukács, G. Fülöp, B. Fülöp, J. Nygård, K. Watanabe, T. Taniguchi, G. Zaránd, and S. Csonka, Observation of spin–orbit coupling induced Weyl points in a two-electron double quantum dot, Commun. Phys. **2**, 108 (2019).

[19] N. P. Armitage, E. J. Mele, and A. Vishwanath, Weyl and Dirac semimetals in three-dimensional solids, Rev. Mod. Phys. **90**, 015001 (2018).

[20] R.-P. Riwar, M. Houzet, J. S. Meyer, and Y. V. Nazarov, Multi-terminal Josephson junctions as topological matter, Nat. Commun. **7**, 11167 (2016).

[21] J. P. T. Stenger and D. Pekker, Weyl points in systems of multiple semiconductor-superconductor quantum dots, Phys. Rev. B **100**, 035420 (2019).

[22] W. Gao, B. Yang, M. Lawrence, F. Fang, B. Béri, and S. Zhang, Photonic Weyl degeneracies in magnetized plasma, Nat. Commun. **7**, 12435 (2016).

[23] A. Bohm, A. Mostafazadeh, H. Koizumi, Q. Niu, and J. Zwanziger, *The Geometric Phase in Quantum Systems* (Springer, Berlin, 2003).

[24] J. K. Asbóth, L. Oroszlány, and A. Pályi, *A Short Course on Topological Insulators* (Springer, Heidelberg, 2016).

[25] K. V. Kavokin, Symmetry of anisotropic exchange interactions in semiconductor nanostructures, Phys. Rev. B **69**, 075302 (2004).

[26] K. C. Nowack, F. H. L. Koppens, Yu. V. Nazarov, and L. M. K. Vandersypen, Coherent control of a single electron spin with electric fields, Science **318**, 1430 (2007).

[27] S. Nadj-Perge, S. M. Frolov, E. P. A. M. Bakkers, and L. P. Kouwenhoven, Spin-orbit qubit in a semiconductor nanowire, Nature (London) **468**, 1084 (2010).

[28] S. Nadj-Perge, V. S. Pribiag, J. W. G. van den Berg, K. Zuo, S. R. Plissard, E. P. A. M. Bakkers, S. M. Frolov, and L. P. Kouwenhoven, Spectroscopy of Spin-Orbit Quantum Bits in Indium Antimonide Nanowires, Phys. Rev. Lett. **108**, 166801 (2012).

[29] M. D. Schroer, K. D. Petersson, M. Jung, and J. R. Petta, Field Tuning the *g* Factor in Inas Nanowire Double Quantum Dots, Phys. Rev. Lett. **107**, 176811 (2011).

[30] P. Harvey-Collard, N. T. Jacobson, C. Bureau-Oxton, R. M. Jock, V. Srinivasa, A. M. Mounce, D. R. Ward, J. M. Anderson, R. P. Manginell, J. R. Wendt, T. Pluym, M. P. Lilly, D. R. Luhman, M. Pioro-Ladrière, and M. S. Carroll, Spin-Orbit Interactions for Singlet-Triplet Qubits in Silicon, Phys. Rev. Lett. **122**, 217702 (2019).

[31] T. Tanttu, B. Hensen, K. W. Chan, C. H. Yang, W. W. Huang, M. Fogarty, F. Hudson, K. Itoh, D. Culcer, A. Laucht, A. Morello, and A. Dzurak, Controlling Spin-Orbit Interactions in Silicon Quantum Dots Using Magnetic Field Direction, Phys. Rev. X **9**, 021028 (2019).

[32] C. Fang, M. J. Gilbert, X. Dai, and B. A. Bernevig, Multi-Weyl Topological Semimetals Stabilized by Point Group Symmetry, Phys. Rev. Lett. **108**, 266802 (2012).

[33] C. Fang, Y. Chen, H.-Y. Kee, and L. Fu, Topological nodal line semimetals with and without spin-orbital coupling, Phys. Rev. B **92**, 081201(R) (2015).

[34] W. Wu, Y. Liu, S. Li, C. Zhong, Z.-M. Yu, X.-L. Sheng, Y. X. Zhao, and S. A. Yang, Nodal surface semimetals: Theory and material realization, Phys. Rev. B **97**, 115125 (2018).

[35] J. Guckenheimer and P. Holmes, *Nonlinear Oscillations, Dynamical Systems, and Bifurcations of Vector Fields* (Springer, Berlin, 1983).

[36] M. V. Berry, Physics of non-Hermitian degeneracies, Czech. J. Phys. **54**, 1039 (2004).

[37] W. D. Heiss, The physics of exceptional points, J. Phys. A: Math. Theor. **45**, 444016 (2012).

[38] J. R. Petta, A. C. Johnson, J. M. Taylor, E. A. Laird, A. Yacoby, M. D. Lukin, C. M. Marcus, M. P. Hanson, and A. C. Gossard, Coherent manipulation of coupled electron spins in semiconductor quantum dots, Science **309**, 2180 (2005).

[39] D. J. Reilly, J. M. Taylor, J. R. Petta, C. M. Marcus, M. P. Hanson, and A. C. Gossard, Suppressing spin qubit dephasing by nuclear state preparation, Science **321**, 817 (2008).

[40] J. R. Petta, H. Lu, and A. C. Gossard, A coherent beam splitter for electronic spin states, Science **327**, 669 (2010).

[41] J. Danon and Yu. V. Nazarov, Pauli spin blockade in the presence of strong spin-orbit coupling, Phys. Rev. B **80**, 041301(R) (2009).

[42] Z. Yan and Z. Wang, Floquet multi-Weyl points in crossing-nodal-line semimetals, Phys. Rev. B **96**, 041206(R) (2017).

[43] S. Ahn, E. J. Mele, and H. Min, Optical conductivity of multi-Weyl semimetals, Phys. Rev. B **95**, 161112(R) (2017).

[44] Z.-M. Huang, J. Zhou, and S.-Q. Shen, Topological responses from chiral anomaly in multi-Weyl semimetals, Phys. Rev. B **96**, 085201 (2017).

[45] T. Souza, M. Tomka, M. Kolodrubetz, S. Rosenberg, and A. Polkovnikov, Enabling adiabatic passages between disjoint regions in parameter space through topological transitions, Phys. Rev. B **94**, 094106 (2016).

[46] Lajos Diósi, *A Short Course in Quantum Information Theory: An Approach From Theoretical Physics* (Springer, Berlin, 2007).

[47] S. Csonka, L. Hofstetter, F. Freitag, S. Oberholzer, C. Schönenberger, T. S. Jespersen, M. Aagesen, and J. Nygård, Giant fluctuations and gate control of the g-Factor in InAs nanowire quantum dots, Nano Lett. **8**, 3932 (2008).

[48] M. Veldhorst, R. Ruskov, C. H. Yang, J. C. C. Hwang, F. E. Hudson, M. E. Flatté, C. Tahan, K. M. Itoh, A. Morello, and A. S. Dzurak, Spin-orbit coupling and operation of multivalley spin qubits, Phys. Rev. B **92**, 201401(R) (2015).

[49] D.-W. Wang, C. Song, W. Feng, H. Cai, D. Xu, H. Deng, H. Li, D. Zheng, X. Zhu, H. Wang, S.-Y. Zhu, and M. O. Scully, Synthesis of antisymmetric spin exchange interaction and chiral spin clusters in superconducting circuits, Nat. Phys. **15**, 382 (2019).

[50] A. Crippa, R. Maurand, L. Bourdet, D. Kotekar-Patil, A. Amisse, X. Jehl, M. Sanquer, R. Laviéville, H. Bohuslavskyi, L. Hutin, S. Barraud, M. Vinet, Y.-M. Niquet, and S. De Franceschi, Electrical Spin Driving by *g*-Matrix Modulation in Spin-Orbit Qubits, Phys. Rev. Lett. **120**, 137702 (2018).